

Atlantic-Type Passive Margin Structural Style of the Cretaceous Basin inNorthern Tunisia: Paleoslope Reconstruction and Regional Tectonics

Ch Naji, Z. Amri, A. Masrouhi, Olivier Bellier

▶ **To cite this version:**

Ch Naji, Z. Amri, A. Masrouhi, Olivier Bellier. Atlantic-Type Passive Margin Structural Style of the Cretaceous Basin inNorthern Tunisia: Paleoslope Reconstruction and Regional Tectonics. Geotectonics, 2022, 56 (1), pp.85-106. 10.1134/S0016852122010034 . hal-03662813

HAL Id: hal-03662813
https://hal.science/hal-03662813

Submitted on 12 Jan 2023

HAL is a multi-disciplinary open access archive for the deposit and dissemination of scientific research documents, whether they are published or not. The documents may come from teaching and research institutions in France or abroad, or from public or private research centers.

L'archive ouverte pluridisciplinaire **HAL**, est destinée au dépôt et à la diffusion de documents scientifiques de niveau recherche, publiés ou non, émanant des établissements d'enseignement et de recherche français ou étrangers, des laboratoires publics ou privés.

Atlantic–Type Passive Margin Structural Style of the Cretaceous Basin in Northern Tunisia: Paleoslope Reconstruction and Regional Tectonics

Ch. Naji [a, *], Z. Amri [a], A. Masrouhi [b], O. Bellier [c]

[a] *Geo-Resources Laboratory, Water Researches and Technologies Center Borj-Cedria and Carthage University, Faculty of Sciences of Bizerte, 7021, Bizerte, Tunisia*

[b] *King Abdul-Aziz University, Faculty of Earth Sciences, Department of Structural Geology and Remote Sensing, P.O. Box 80206, Jeddah 21589, Saudi Arabia*

[c] *Aix Marseille University, CNRS, IRD, INRAE, CEREGE, BP80, 13545 AIX en Provence, CEDEX 04, France*

**e.mail :chahreddine.naji.geo@gmail.com*

Received October , 2021 ; Revised November 17, 2021;

Abstract – The purpose of this paper is to characterize the configuration of northern Tunisia's basin during the Cretaceous on the basis of abundant slump folds and frequent synsedimentary faults. The slump folds are studied to determine the slumps transport vergence on the synsedimentary submarine paleoslope. The local and regional stress field is used to characterize the syn-sedimentary deformation. During Valanginian–Aptian times, the basin is characterized by southward submarine slope. From Albian to Santonian times, the slump folds analysis provides a NNW- to NW-ward sloping topography. The fault kinematic analysis reveals a regional NW- to NNW-trending Cretaceous tectonic extension. Locally, a NE- to N-trending extension is characterized. A perturbation of paleoslope orientation is locally observed probably related to salt tectonics hyperactive during Aptian–Albian. The constructed regional cross-section shows a tilted block geometry governed by major basement faults associated to other intra-basin growth faults. The basin shows a ±5° seaward facing submarine paleoslope. In addition, some structures are probably dominated by raft tectonics.

All these features are fairly consistent with the conclusion that the basin is very similar to the present-day Atlantic–type passive margins.

Keywords: Cretaceous, soft-sediment deformations, slumps, paleoslope, faults, tectonics, passive margin, Tunisia

INTRODUCTION

Submarine slumping is considered to be the most common feature of large-scale gravity-driven sediment deformations. This deformation feature can result from the interplay of instabilities related to slope failure, rheology changes and sediment layering. Commonly, soft sediment deformations are recognized particularly in rifts and passive margins contexts [2, 3, 4, 6, 29, 89, 95, 100]. During and/or after sedimentation, non-cohesive or poorly lithified sediments are translated along the slope (usually from the continental shelf to the basin) to generate a wide range of gravity driven structures in successive depositional events. That is why the investigation made on the genetic relationship between the slope attitude and the triggered slumping was the subject of lengthy debates [6, 24, 49, 50, 89, 90, 98, 100].

Generally, these investigations made on soft-sediment slump sheets perceive them as gravity driven cells, which systematically reflect downslope orientation. Hence, the examination of slump folds yields a potential opportunity to drawback many meaningful structural interpretations and paleogeographic reconstructions [24, 50, 90, 100].

Many techniques have been designed to determine the paleoslope dip direction from slump sheets. These techniques are based on the systematic relationship with slope attitude upon which they were primarily triggered. The mean axis method (MAM) was the first approach applying this idea. Jones [49, 50] suggested this method, which received the greatest application. This method is based on the assumption that the mean slump fold axis seems to be normal to the flow orientation. More recently, the study of soft-sediment deformations

received more and more attention and other techniques have been described to infer paleoslope vergence from the analysis of slumped sediments [5, 6, 19, 24, 25, 98–100]. These techniques use various slump folds components including the fold axis, the axial plane and the interlimb angle [2].

Northern Tunisia includes numerous localities that expose abundant soft-sediment deformation features and exceptional Cretaceous slump-sheet horizons (Fig. 1). The genesis of this latter is crucially related to the geological evolution of the southern Tethyan rifted continental margin. Soft-sediment deformations structures remain insufficiently characterized or even unstudied in the aforementioned area, and the basin geometry and its evolution are still debated.

Various are the purposes behind this present paper. To begin with, the fundamental aim is to apply the paleoslope determination approach from slump folds to the North African passive paleomargin. Another important goal is to determine the tectonic regime during Cretaceous from fault kinematic analysis. This study is based on lithostratigraphic correlations which allow the assessment of facies and thickness variations along the study area.

This paper is an extension of the previous synthetic work that allowed documenting the connection between the slump folds and the basin' submarine paleoslope [72, 73]. The present contribution aims to enlarge the area of investigation throughout the north Tunisian Atlassic domain.

The present work introduces some other new techniques. In addition to the previous purposes, this study intent is to combine all obtained datasets from various approaches to drawback the structural configuration of the north Tunisian basin during the Cretaceous in relationship with the evolution of the Tethyan passive paleomargin.

GEOLOGICAL SETTING

Meso-Cenozoic structural evolution of northern Tunisia

The Atlas chain extending from the western Atlantic coasts of Morocco to the eastern coasts of Tunisia represents a part of the Alpine chain of Africa. The northern Tunisian domain corresponds here to the northeastern part of the southwest-northeast trending Atlas fold and thrust belt system (Fig. 1). This chain is formed during the Cenozoic Alpine orogeny associated with Africa and Eurasia convergence [16, 30, 43, 53, 57]. In Tunisia, the northern Atlas system is usually divided into two structural units [32, 61, 75, 97] (Fig. 1):

– the first unit, to the North, is known as the southeastward Teboursouk thrust unit and located in the Tunisian part of the northeastern Maghreb salt province. It exhibits thick Aptian–Albian deposits disturbed by abundant outcropping salt structures;

– the second unit corresponds to the Zaghouan–Ressass thrust unit, bounded to the south by the present-day Zaghouan thrust fault. This latter has been described during Cretaceous as a major paleogeographic structure separating the northern deep basin from the southern shallow zone [42, 52, 94].

The Mezo–Cenozoic tectono-sedimentary evolution in Tunisia shows two main periods of deformation. The first one corresponds to the Tethyan and the Atlantic oceans opening. This stage, from rifting to passive continental margin, was initiated approximately during Late Triassic–Early Jurassic and persists until the Early Cretaceous [31, 44, 76]. It was responsible for the setting-up of Triassic basin largely filled with evaporitic deposits across the major part of Tunisia [51, 88]. As a result, during Jurassic and Early Cretaceous, a major extensional regime prevailed and was accompanied in some northern Tunisian localities with volcanic and halokinetic activities [7, 10, 18, 46, 66, 88]. From Early to Middle Albian seems to coincide with the final stage of the Atlantic Ocean opening [45]. During Aptian–Albian, the basin underwent rapid extension [65, 72]. Thus, numerous Cretaceous salt movements attest of the more intense, mixed thick-and thin-skinned extension [7]. Concomitantly, the major syn-

sedimentary faulting draws a general tilted blocks configuration controlling the irregular sea-floor [46, 73, 84, 87]. These blocks are characterized by high sedimentation rate, ample slumps folding and abundant syn-tectonic sequences [45, 46, 58, 73]. Unlikely, the Late Cretaceous period is perceived here as a post-rift stage since it is mainly dominated by homogenous carbonate and open marine shale facies [82]. Following this Mesozoic rifting, the second main phase, due to African/Eurasian plate's convergence, induces the closure of the Tethys seaway [16, 27, 43]. Subsequently, two major compressional tectonic events seem to be recorded in Tunisia from Late Cretaceous to present-day time [52, 53, 54, 60]:

– the first event corresponds to the Atlassic compressional event which led to the closure of several Mesozoic basins during the middle to late Eocene;

– the second event is correlated to the middle Miocene Alpine compression and represents the major orogenic contractional event in Tunisia.

The second tectonic event is considered to be a key factor for the establishment of the present-day NE-trending complex northern Tunisia orogen [35, 54, 65]. It is also important to note that the alpine compression is recognized to be still active until present-day time [11, 34].

Cretaceous lithostratigraphy of northern Tunisia and correlation of the studied sections

In northern Tunisia, the Jebel Oust locality situated a few kilometers to the north of the Zaghouan town, is considered to be the reference type-section of Early Cretaceous basin sequences [13, 73, 87] (Fig. 1). In fact, this locality exposes Berriasian–Aptian basin series which are estimated to reach more than 2500 m-thick. The Tithonian–Berriasian marly series is mainly composed of mud and debris flow deposits succeeded by thin-bedded siltstones and sandstones. The Valanginian deposits, usually referred to as the Seroula Formation [87], are mainly consisted of siliciclastic turbidites and slumped quartzite beds overlain by Hauterivian

series. These latter are made up of mixed shelf sequences topped by siliciclastic and carbonate storm deposits with marls suggesting a platform facies. The Hauterivian sequences are covered by the Barremian series which began with mixed tempestites and slumped sandstone horizons. The upper Barremian unit is marked by large black shales sequences [87]. In the same locality, the Aptian–Early Albian deposition, with black marls and limestones, is believed to have occurred under deeper water. The Hauterivian–Aptian deposition in Tunisia is attributed to the M'cherga Formation [20]. In northern Tunisia, the Albian–Cenomanian Fahdene Formation is made of deep-water facies [20]. These sequences expose gray to black marls alternating with abundant metric to decametric limestone beds. Over Fahdene Formation, rest thinly laminated organic rich black shales; these are defined as the Uppermost Cenomanian–Early Turonian aged Bahloul horizon [20, 85]. On top of this reference horizon lie gray shale and marls alternating with micritic limestone beds, all affiliated to the Aleg/Kef Formation defined as Turonian–Early Campanian [20]. This formation is topped by the Late Campanian–Early Maastrichtian Abiod Formation, which is essentially composed of two fine-grained limestone bars intercalated by marl-limestone alternations. All are overlain by the Maastrichtian–Paleocene-aged El Haria Formation.

During Late Cretaceous, the siliciclastic and detrital deposits are well restricted and the sedimentation becomes more and more uniform with pelagic to hemi-pelagic sequences. As a result, Late Cretaceous sequences show highly homogeneous facies distribution composed of marls associated with white limestone beds [13].

An 85-km–long correlation of the Late Cretaceous series of northwestern Tunisia is drawn from the Jebel Ballouta-Serj-Bargou area in the southeast, to the Nebeur–Mellegue area to the northwest (Fig. 2). It is based on existent lithostratigraphic sections collected from previous works that are slightly modified in the current study. This lithostratigraphic correlation shows no significant facies variation but it sheds light on a considerable thickness change. The

Zaafrana and Nebeur sections belonging to the Kef basin show thick Cenomanian–Maastrichtian sequences compared to the Bled Doghra restricted section. Similarly, the Serj-Bargou section seems to be a depocenter with high rate of sedimentation during Late Cretaceous times. In addition to the thickness variation, the measured sections highly exhibit abundant nodule reworking, numerous slump sheets, olistholites blocks and conglomeratic layers.

APPROACH AND METHODOLOGY

The tectono-sedimentary architecture of the North Tunisian basin is interrelated to the structural evolution of the Tethyan margin. Thus, our study is based on slump transport determination and kinematic analysis of fault datasets that exhibit main information about the brittle and hydroplastic deformations related to the basin expansion during Cretaceous times.

Accurate field sections, numerous slump folds and fault populations were measured. Field datasets were processed with different software. For plotting and analysis of slump and fault datasets, Stereonet 9 [1] and Win-Tensor [26] software were used. The data out draft and design were made using the Canvas drawing software. Field work focused on the slump folds, which allow the orientation drawback of the syn-depositional slope, and the syn-sedimentary faults, which yield significant information related to the original tectonic regime.

The Fault kinematic analysis method was mobilized to quantify the brittle deformation. Such analysis permits the quantitative restoration of paleostresses which yield significant information on the extensional, compressional or strike-slip origin of deformed structures [77]. The paleostress regimes were reconstituted in the light of the analysis of mesoscale fault slip data sets. These sets are collected in the field and include the fault plane dip and direction, and measurement of the associated striae. The syn-sedimentary fault populations have been specifically surveyed, because they directly provide the date of the tectonic event.

In some cases, the measured fault mirrors have, not only one set of striation. In such case, distinct striae populations have been distinguished based on structural arguments using the relative chronological record (crosscutting relationships). The numerical processing of fault populations was made according to the Right Dihedron method [8, 91] and the Optimum methods [26]. These methods allow the reconstitution of reduced stress tensor, i.e. the directions of principal stresses ($\sigma1 \geq \sigma2 \geq \sigma3$), and the stress ratio $R = (\sigma2-\sigma3/\sigma1-\sigma3)$. As a result, we can deduce three tectonic regimes which can be distinguished in regard to the vertical principal stress, i.e. extensional tectonic regime is outlined by vertical σ1, compressional regime is given by vertical σ3 and strike-slip regime is characterized by vertical σ2. Accordingly, this calculated stress tensor reveals evidence of a local state of stress. In order to reconstruct the original stress tensors, fault datasets need to be rotated to their horizontal orientation. The study area exposes abundant faults showing well preserved tectonic indicators in which fault movement and type are well expressed on fault mirrors. Thus, to optimize the structural interpretation, a significant number of striated fault populations ranging from Albian to Santonian age, is processed.

The orientations of slump folds have been regarded to be tightly correlated with the submarine paleoslope dip direction (Fig. 3a, b). Therefore, several techniques allowing the determination of the paleoslope orientation from slumps distribution have been already developed. Jones [49, 50] was the first to apply the structural relationship between slumps folds and paleoslope attitude. Recently, other studies have described a variety of statistical techniques to determine the syn-depositional slope orientation from these gravity driven slump sheets [2–6, 19, 24, 25, 89, 90, 98–100]. Our approach is to conduct a rigorous paleoslope reconstitution by means of two methods (Fig. 3c):

– the Mean Axis Method (MAM);

– the Axial-Planar Method (APM).

The Mean-Axis Method (MAM)

The MAM, originally established by Jones [49, 50] and updated by Woodcock [99], assumes that slumps fold axes are systematically parallel to the paleoslope and normal (perpendicular) to the flow of slump sheet. Consequently, this method yields two diametrically opposed transport directions (Fig. 3c). The most probable direction is usually defined by geologist on the basis of the regional consideration and field checks (paleogeography, probable deepening of the basin, vergence of the folds, shear features). These slump folds data, or at least the obtained paleoslope orientation, needs to be restored to their original direction before folding, by removing the subsequent compressional tectonics.

One disadvantage of the MAM is that it is statistically vigorous as it is founded on the mean of slump fold measurement data. The main deficiency of the MAM is that it does not consider the downslopes where fold axes are driven parallel or oblique with respect to the flow orientation [49, 50, 100].

The Axial Planar Method (APM)

The Axial Planar Method (APM) is based on the fold axial surfaces (in use as planes) that provide meaningful kinematic evidences in analogy to fold axes [98, 99]. According to the APM, poles to axial planes tend to align in a great circle around the mean fold axis (Fig. 3c). Subsequently, the best-fit girdle strike to these poles gives a bidirectional estimation of the slumps sheet direction [3, 99]. In addition, the vergence of the mean axial plane considering the general slumps flow direction is used to infer the syn-depositional slope dip direction [99]. These methods are considered to be the most suitable to our study area, where layer-parallel shear was dominated and little sub-sequent fold rotation has induced.

SYNSEDIMENTARY FAULTING ANALYSIS

(EL-KEF AND SILIANA REGIONS)

Field investigation has been performed to measure fault planes, thus delivering significant reports about the paleostress tectonic regime. The study area (El Kef and Siliana regions) displays evidence for well-preserved tectonics indicators on numerous syn-sedimentary fault planes (Fig. 4, Fig. 5). Hence, syndepositional striated faults are especially surveyed. Consequently, a wide range of fault datasets is compiled from Jebel Serj-Bargou-Ballouta and Zaafrana regions aiming to infer the tectonic regime during Albian, Cenomanian–Turonian and Coniacian–Santonian times.

Tectonic regime

Albian. In northern Tunisia, Albian layers expose frequent conglomeratic horizons and slump sheets associated with considerable thickness changes [45, 47]. The Albian deposits reviewed under the current study exhibit numerous meso-scale sealed normal faults that originally trend ~NNW–SSE and ~N–S. Fault measurements were carefully collected from Albian sequences ofthe Jebel Bargou structure (Oued El Kharroub section) and then rotated to their initial strike and dip to reconstruct the former stress field.

Jebel Bargou is located in the Southeast of the study area between Siliana and Oueslatia (Fig. 6). This anticline structure shows large geological series extending from Aptian to Quaternary and mainly affected by N140 and N070 trending faults delimiting various blocks [12, 86, 93]. Two sites, located in Oued El Kharroub section showing large Lower Cretaceous series, reveal consistent NNE-trending extensional regime during Albian time:

- the first site indicates a clear extensional tectonic regime, for which stress tensor shows horizontal NNE-trending σ3 (Fig. 6, S1_1).
- the second site expresses an extensional tectonic regime with very close stress tensor (Fig. 6, S2_1).

Cenomanian–Turonian. Most of the analyzed Cenomanian-Turonian faults reveal that the predominant stress regime in northwestern Tunisia corresponds to NW to WNW-trending pure extension. The Cenomanian–Turonian fault dataset was collected from Serj–Bargou area; it is a large NE-trending structure along the Zaghouan–Ressas zone.

The Jebel Serj structure is situated a few kilometers to the southeast of the Bargou structure. Jebel Serj is a NE-oriented anticline structure with a collapsed northern limb. The flexure is drawn in the Aptian limestone of Serj Formation defined originally in this locality. On a larger scale, this structure is affected by ENE- to NE-trending faults [93]. The present survey hand in hand with the previous works confirms a considerable westward thickening of the Late Cretaceous series of the southern limb of Serj anticline [92, 93, 94]. Furthermore, Cenomanian deposits from the southern limb of this structure show numerous soft-sediment deformations such as slump folds and olistholites blocks (Fig. 4b).These syn-depositional features attest for sedimentation above sloped basin floor related here to normal faulting acting during and/or probably before this period. On a mesoscale, abundant sealed faults are observed, from which the deduced stress tensors reveal a rather homogenous stress state along the field area. In details, four sites measured from Cenomanian strata of the southern limb of Serj structure exhibit a tectonic regime with a general NNW to NW-trending extension during this period (Fig. 6, S1_2, S2_2, S3_2 and S4_2). The first two sites yield a stress tensor indicating a NNW-SSE horizontal minimum stress axis σ3 (Fig. 6, S1_2 and S2_2). Similarly, the third and fourth sites show a close extensional paleostress regime marked by a NW-trending horizontal minimum paleostress axis (Fig. 6, S3_2 and S4_2). The last site was analyzed from the Cenomanian deposits of the northern limb of Jebel Bargou (Oued El Kharroub locality). After processing, the pre-tilted stereoplot of this site illustrates a similar sub-horizontal NW–SE σ3 (Fig. 6, S7_2).

Other paleostress tensors were calculated from the Uppermost Cenomanian–Early Turonian aged Bahloul Horizon of the Oued El Kharroub locality on the northern limb of Jebel Bargou structure. This area exposes numerous sealed synsedimentary normal faults (Fig. 4a). The uppermost part of the Bahloul horizon is marked by numerous Cenomanian–Turonian olistolith blocks indicating syn-depositional tectonic activities [9, 86] (Fig. 4a). From this reference horizon, four sites have been chosen for fault measurement. After rotation to the original orientation, they show homogenous NNW–SSE to NNE-trending extensional tectonic regime (Fig. 6, S5_2, S6_2, S8_2 and S9_2). More precisely, the back-tilted fault stereoplots of the first three sites show sub-horizontal minimum stress axis σ3 that trends NNW (Fig. 6, S5_2, S6_2 and S8_2). On the other hand, the last fault population collected from the same horizon reveals sub-horizontal NNE-trending σ3 axis (Fig. 6, S9_2).

Coniacian–Santonian. In northwestern Tunisia, frequent remarkable synsedimentary extensional features are exposed in the Coniacian–Santonian sequences. Numerous are the Coniacian–Santonian normal faults which are collected from Jebel Serj-Ballouta and Zaafrana regions (Fig. 5). Thus, an extensional tectonic regime deduced from fault-slip data sets is considered to be highly predominant in all sites.

The Coniacian-Santonian deposits of the Serj-Ballouta structure show abundant striated normal fault populations (Fig. 5c, d, e). Following data processing, the back-tilted fault diagrams collected from these sequences show general ~ENE to ~NNE-trending extensional tectonic regime (Fig. 6, S1_3, S2_3, S3_3, S4_3 and S5_3). This is believed to be significantly homogenous in the whole area.

The paleostress tensor computed from the first site delivers near horizontal NNE–SSW minimum stress axis (Fig. 6, S1_3). Similarly, the second site collected from the same region characterizes a pure extensional regime with gently plunging NE–SW σ3 (Fig. 6, S2_3). Likewise, the following site collected from the same area displays extensional NNE-trending

paleostress tensor (Fig. 6, S3_3). Exceptionally, the fourth site suggests a little different result with sub-horizontal NNW-trending σ3 stress tensor (Fig. 6, S4_3). Unlikely, the last fault population is illustrated by the back tilted fault diagram S5_3 in Figure 6, which suggests an ongoing extension with ENE–WSW horizontal minimum stress axis.

Another locality, from which some other fault datasets were collected, is defined as the Zaafrana area. This NE-trending folded zone is located in the southeast of the El Kef area. The Zaafrana area exposes the Zaafrana Coniacian-aged core anticline in the southeast, and the Dyr El Kef Eocene-aged core syncline in the northwest. To the South, this structure is limited by the large Nadhour syncline. The thick Coniacian-Santonian series (~1000 m of thickness) is composed at the base by marl-limestone alternations and large gray marls at the top exposing frequent synsedimentary normal faults (Fig. 5a, b). Five sites calculated from the Zaafrana area show homogenous stress field during Coniancian–Santonian times (Fig. 7, S6_3, S7_3, S8_3, S9_3 and S10_3). Subsequently, the resulting back-tilted fault diagrams display homogeneous minimum stress axis σ3 with general ~ENE to ~NE -trending during this period.

To be more precise, the pre-tilted fault diagram of the first site illustrates ~ENE extensional paleostress regime (Fig. 7, S6_3). As shown in the figure provided, the paleostress tensor computed from the second site commonly provides sub-horizontal NE-SW trending minimum stress axis (Fig. 7, S7_3). Besides, the third site located in the same area confirms the extensional tectonic regime (Fig. 7, S8_3). The measured parameters indicate sub-horizontal minimum stress axis (σ3) trending always NE–SW. The following site also exhibits the extensional regime (Fig. 7, S9_3). Thus, the corresponding back-tilted fault diagram provides horizontal minimum NNE–SSW stress axis. The last site of fault population suggests pure extensional paleostress tectonic regime marked by an almost horizontal ENE-trending stress tensor (σ3) (Fig. 7, S10_3).

REGIONAL STRESS REGIME AND TEMPORAL EVOLUTION OF THE DEFORMATION

The determination of the regional stress state is believed to be highly significant to understand geological records of the studied structures and their genesis in relation to plate tectonics. Striations measured in the above-mentioned faulted area were used to quantify the regional stress regime in the study area. The efficiency of the local fault populations is sometimes disturbed by major preexisting faults or diapir growth. For this, a regional stress regime is calculated. To do so, graphical methods have been used to separate heterogeneous datasets and eliminate non-linear measurements. This approach gives quite reasonable results in the case of studying young deformations in a small geological area [8, 91]. In more complex cases, another approach is presented when separating the initial data of seismological and geological indicators of discontinuous displacements [77, 78, 79]. Besides, the regional stress state in the present work is statistically based on major fault data according to the right dihedron method and/or optimum methods in order to estimate the temporal evolution of the tectonic deformation.

From Albian to Santonian time, northwestern Tunisia seems to be controlled by a persistent extensional tectonic regime related to the Cretaceous rifting. The inversion of eight Albian-aged major striated faults, usually sealed by limestone beds, indicates NNE-extensional regional regime with strike-slip components. In fact, the corresponding back-tilted faults diagram illustrates horizontal NE-trending minimum stress tensor σ3 (07/035) and R=0.94. The high angle WNW–ESE (83/213) σ1 axis and horizontal σ2 (00/305) and σ3 (07/035) define a pure NE–SW tectonic extension (Fig. 8a). During Cenomanian, the unfolded major faults diagram clearly illustrates a NW-trending extensional tectonic regime according to the parameters obtained from 15 fault data inputs. Subsequently, the regional Cenomanian stress

tensor shows horizontal NW–SE (03/132) σ3, horizontal (06/042) NE–SW σ2 and high-angle plunging (83/248) ENE–WSW σ1. This fault population shows R=0.4 (Fig. 8b). Furthermore, 12 measurements are processed from major faulting collected throughout the Bahloul horizon dated as Uppermost Cenomanian–Lower Turonian. These fault populations exhibit NNE-extension with strike-slip components. Thus, the back-tilted fault stereoplot shows a sub-horizontal minimum stress axis σ3-trending NNE (16/006) and a gently plunging WNW–ESE σ2 (06/098). This site shows a stress tensor with NNE–SSW subvertical σ1 (73/208). It should be also noted that the determined stress ratio is R=0.88 (Fig. 8c). Besides, Turonian regional stress regime is also highlighted from the kinematic analysis of 11 major normal fault systems. A pure NNW-extension is deduced during this period. The computed paleostress tensor provides an ENE–WSW σ2 (72/263), a near horizontal NNW–SSE σ3 (04/159), and a gently plunging ENE–WSW σ1 (17/068). The processed fault measurements reveal a stress ratio R=0.54 (Fig. 8d).

The last regional stress state is calculated from 21 large-scale sealed faults collected from Coniacian-Santonian sequences. The back-tilted fault diagram shows gently plunging NNE–SSW σ3 (10/198), near-horizontal WNW–ESE σ2 (01/288) and high-angle plunging NNE–SSW σ1 (80/024). This diagram provides R=0.56. Consequently, all of the mentioned criteria suggest a pure tectonic extension which trends NNE–SSW (Fig. 8e). This fault diagram clearly shows two heterogeneous families of fault populations that may reflect two distinct extensional tectonic events. Consequently, through the graphical separation of these different fault datasets, the first unfolded fault population exhibits a pure NNE-trending extensional regime in regards to the following parameters of the stress tensor: a sub-horizontal plunging NNE–SSW (04/214) σ3, a gently plunging WNW–ESE (07/123) σ2 and a high-angle plunging NNW–SSE (82/330) σ1. This fault population exhibits a stress ratio R=0.53 (Fig. 8e, (1)). Whereas, the second separated fault population displays a horizontal NNW-trending

minimum stress tensor σ3 (04/154) and a stress ratio R=0.5. The σ1 axis of this stress regime has high angle trending ENE–WSW (59/057) and the intermediate σ2 stress trends ENE–WSW and shows 31/246 stress axis (Fig. 8e2). This last faults population seems to be older compared to the first one because its relative back-tilted faults diagram displays results close compared to the Turonian stress tensor (Figs. 8e, (2), 8d).

SLUMPS ANALYSIS RESULTS

More than 80 slump folds were measured from various localities in northwestern Tunisia. Early Cretaceous slumps folds were measured from the Jebel Sidi-Amor structure located northeast of the Nebeur area. Other Albian-aged slump features are collected from Oued El Kharroub situated in the northwestern limb of Jebel Bargou anticline. In the same way, 14 Cenomanian-aged slump features were measured in the southern limb of the Jebel Serj structure. Besides, more than 40 slump features were collected from Coniacian–Santonian deposits of Zaafrane area, Bled Doghra, Jebel Lorbeus and Jebel Serj-Ballouta structure.

In the study area, Early Cretaceous series are mainly dominated by marly sequences highly affected by extensional tectonics testifying of a sub-marine sedimentation above an unstable basin floor. Under the aforementioned conditions, the irregularity of the basin floor (slope) coupled with high rate of sedimentation may generate slumping sheets within deposits before their own lithification. Thus, numerous slump folds have been recognized across the studied sections in the light of several criteria. These latter allow the distinction of these gravity driven deformations from micro and/or mesofolding generated due to tectonic contractions. The major robust difference is related to the preexistence of axial planar cleavage in tectonic folds, compared to its absence in soft-sediment folding [6]. The second reliable criterion indicating slumping is illustrated by the interbedding of the slump sheets between two un-deformed layers and the presence of erosional surface at the top of the sheet and an

underlying detachment plane at the base [5, 50, 98]. Another main difference between two types of folds (tectonic folds and slump folds) can be highlighted on the assumption that during gravity-driven slumping, compression is always associated with extensional deformation, whereas during tectonic folding, it is directly connected to the process of compression [74]. In addition, other criteria are involved by Elliott and Williams [28] to describe ductile slump folds such as distorted and overturned strata, thickening and thinning of strata, striated and sometimes detached slump folds, rolled up and chaotic fragments of strata near the slump sheet [28].

In the Jebel Sidi Amor locality (Nebeur region), 14 slump folds were carefully measured and were documented throughout Valanginian-Hauterivian siliciclastic carbonates deposits. A range of slump fold shapes (open folds to steeply inclined ones) was observed in this section (Fig. 9b, c, (1)). The back-tilting datasets of different scales measured slump folds using MAM and APM methods clearly display very similar results, with general ~south dipping paleoslope. Therefore, these methods display respectively ~N193 and ~N189 trending paleoslope (Fig. 9a, (1)).

The Albian epoch is accepted to be the most important regional extensional period during the Mesozoic rifting in this area [33, 46, 63, 87]. In the Oued El Kharroub section, 8 slump fold structures were rigorously measured within green-black marls intercalated with thin marly limestone beds classically attributed to Fahdene formation. Thus, these slumping sheets expose metric to decametric scale folds with obtuse interlimb angle geometry (Fig. 9a, (2)). While the measurement of Albian unfolded slump axis (MAM method) exhibits ~N352-trending paleoslope, the rotated poles of axial planes (APM method) display analogous value of a ~N354-trending paleoslope (Fig. 9b, (2)).

15 km to the southwest, Cenomanian deposits of the southern limb of Jebel Serj anticline are wholly formed by gray marls and shales alternating with micritic limestones (Fig. 10a). This

succession is overlain by the organic rich platy limestones of the Bahloul horizon, attributed to the Uppermost Cenomanian–Early Turonian [9, 85]. In this locality, from east to west, the Cenomanian series clearly show a considerable westward thickening that was probably related to synsedimentary normal faulting activity. These sequences exhibit well preserved meso-scale slump features associated with numerous soft-sediment deformations (olistoliths, reworked calcareous nodules and conglomeratic layers). Consequently, abundant metric olistostromes and frequent reworked blocks are believed to be inferred from gravity sliding along a submarine paleoslope. In this area, 14 slumps were measured and their analysis shows a persistent ~NW-downslope transport. The rotated slump axis (MAM Method) provides a ~N316-trending paleoslope and the restored poles of axial planes (APM method) attest a similar paleoslope direction with ~N320-trending (Fig. 10b).

In the entire northern Tunisia domain, the Coniacian–Santonian sequences are mainly made of thick sequences of gray marl and shale embedded with micritic limestones. In northwestern Tunisia, these deposits also display evidence of frequent gravity driven structures classified as soft-sediment deformation.

Throughout the Zaafrana section, Coniacian strata expose abundant slumps features and frequent calcareous nodules associated with numerous decametric normal faults (Fig. 11a, b, (1)). The analysis of the slump folds collected from the Coniacian-Santonian sequences always gives a general NW-downslope transport orientation. In more details, the MAM and APM methods provide ~N319 and ~N322-trending paleoslope, respectively (Fig. 11c, (1)).

20 km to the southeast, the Bled Doghra locality is a 5 km^2 salt structure described as a submarine allochthonous salt sheet, formed during Early Cretaceous [63]. The oldest outcropping series in contact with the Triassic rocks corresponds to the Albian deposits [63]. In the western portion of this structure corresponding to the Oudiba anticline, the Triassic salt is exposed under a 1–2 m thick conglomeratic horizon composed of coarse Triassic insoluble

elements parallel to the planar disposition of Triassic material [63]. This horizon is covered by stratified dolomitic layers which show considerable thickness change ranging from 10 m at the Choua River to ~100 m in the Oudiba mine area [63]. This remarkable thickness variation is interpreted as indicative of sedimentation above a topographically rugose or undulating salt sheet [63]. This dolomitic unit is covered by gray Coniacian-aged marls with numerous soft-sediment deformation structures (Fig. 11a, (2)) usually reflecting sedimentation over a submarine slope. Using MAM and APM methods, the analysis of collected slump folds clearly exhibits a general ~WNW-dipping paleoslope of the basin floor during Coniacian-Santonian times. The unfold axis method suggests a ~N291, and, the unfold poles of axial planes illustrate ~N294 trending paleoslope (Fig. 11b, (2)).

Furthermore, to the southeast, Jebel Lorbeus is interpreted as being a large diapir structure located a few kilometers to the northeast of the Sers plain. This structure exposes Coniacian-Santonian deposits that are characterized by metric to decametric scale slump folds associated with conglomeratic layers and calcareous nodules which are classified as soft-sediment deformations (Fig. 12b, (2)). Computed slump geometric data collected from the northern limb of the diapir structure attest a general NNE-downslope transport direction. Accordingly, the paleoslope orientation derived from MAM and APM methods are ~N018 and ~N019, respectively (Fig. 12a, (2)). However, this disturbed paleoslope orientation seems to be explained by the local topography related to the diapir activity.

Coniacian–Santonian series in the Jebel Serj-Ballouta structure are also composed of thick marly sequences interbedded with micritic limestones. Like Cenomanian strata, the thickness of these series significantly varies from tens to hundreds of meters from the northeast to the southwest. This considerable variation is explained by synsedimentary normal fault activities with an obvious field imprint given by syntectonic deposits, breccia and growth strata geometry. Coniacian–Santonian sequences of this area show abundant soft-sediment

deformations and abundant open hinge mega-slump folds with obtuse interlimb angle associated with frequent extensive synsedimentary features (Fig. 12b, c, d, (1)). The analysis of 14 mega-slump folds attests a persistent general northwestward submarine slope. The rotated axis method exhibits a paleoslope trend of ~N310, and the unfolded poles of axial planes provide ~N312 (Fig. 12a, (1)). The Albian-Santonian persistent northwestward paleoslope apparently attests for a major NE to ENE-trending inherited fault positioned just south to the Ballouta-Serj-Bargou complex structure. This major fault seems to have controlled the Cretaceous sedimentation in these localities, and may be a branch of the large-scale Zaghouan fault.

RESULTS AND DISCUSSION

The examination of soft-sediment deformation in various localities from northern Tunisia during Cretaceous time reveals the basin's submarine paleoslope using slump folds data and the tectonics regimes using fault kinematic analysis. Furthermore, the correlation drawn in the study area clearly reflect considerable thickness variations of the Cretaceous series related to synsedimentary normal faults activity probably responsible for tilted blocks basin geometry [9, 15, 23, 58, 63, 64, 73, 86].

Valanginian–Hauterivian sequences clearly reflect deep marine environments and show abundant intercalated siliciclastic deposits associated with frequent slump sheets. Using the MAM and APM methods, a general southward paleoslope associated with a general ~N–S-trending extensional tectonic regime is highlighted for this period. This southward dipping slope may be explained by the tilted blocks geometry which allows two possible transport directions which are dramatically opposed. The Aptian–Albian period shows significant thickness variation coupled with abundant normal faulting and hyperactive salt tectonics. The fault kinematic analysis here displays evidences for -NNE to NE-trending extensional tectonic

regime that prevailed during Aptian–Albian times. Besides, the rotated slump axes and the poles of axial planes provide a NNW-verging dominant paleoslope. These results raise the problem of oblique extension in regards to the basin evolution. This fact is probably explained by the crucial role of the inherited major faults (with a NE to ENE-trending) which are reactivated during Aptian–Albian period under a NNE-trending tectonic regime.

We find it obvious that these observations emphasize an architecture of rifted continental passive margin characterized by deep listric normal faults associated to abundant soft-sediment deformations and high rate of sedimentation related to increased basin subsidence. During Cenomanian times, high sedimentation rate is perceived followed by facies homogeneity, coeval with decreasing of salt tectonic activity in comparison with the Aptian–Albian period [61]. The thickness variations of the Cenomanian deposits are well correlated to normal faults activity [9, 92]. Using the fault kinematic analysis, a pure extensional tectonic regime with NW-trending extension is proposed. Moreover, a NW-verging related submarine paleoslope is inferred from the unfolded slump axes and poles of axial planes. Concerning the Turonian stage, it is recognized in north Tunisia as black-shales source rocks with homogeneous facies on the entire basin. This fact indicates that the basin is getting deeper. From Cenomanian to Turonian, a probable reorganization of the basin seems to be happening with a tectonic regime that oscillates between NNW- and NNE-trending main regional extensions. The Coniacian–Santonian sequences are mainly made of pelagic to hemi-pelagic slumped large sequences that appear to seal major faults in the basin. Accordingly, the basin is believed to be in a post-rifting subsidence stage during the Coniacian–Santonian times. Based on the analysis of slump folds collected from these series, general paleoslope oscillating between NW- and NNE is deduced. Concerning the kinematic analysis of the Coniacian–Santonian striated fault planes, two successive regional extensional regimes are evidenced with respectively NE and NW orientations. If the first one is attributed to

Coniacian, the second one is admitted as Santonian based on cross-cutting relationship observed in the field.

The Cretaceous paleotectonic blocks' geometry in northern Tunisia is complex and has been misreported in the literature. Rare are the previous studies which targeted the regional compartmentalization of northern basin of Tunisia with regards to the southern Tethyan margin framework [13, 22, 46, 73, 84]. These non-advanced interpretations are also due to the fact that the basin characteristics were disrupted and overprinted by the Tertiary Alpine compressions [65] .Taking into consideration the previous studies, a schematic cross section of the Cretaceous basin in northwest Tunisia has been constructed (Fig. 13). This section is built on the basis of the large number of detailed field surveys of different tectonic blocks (according to our obtained data sets), the thickness of sequences [20, 67, 81], the trace of the major fault systems from the detailed geologic map of Tunisia (Geological survey of Tunisia maps at 1:50000 scale [36–42]) and the salt tectonics. At depth, the cross section is constructed based on the assumption that the ductile stretching of the lower crust is greater than the brittle extension of the upper crust [17]. The geometry of each block is drawn following the paleoslope reconstruction itself inferred from slump folds analysis. Furthermore, the crustal thickness, the continental lithosphere and the Moho depth are all constructed based on several studies [48, 71, 80].

During the lowermost Cretaceous, the N-trending regional tectonic extension seems to be the continuation of the Jurassic regime. In the North African domain, the Jurassic period is well highlighted as an active rifting period as well as in Tunisia [10, 18, 59, 65, 69, 70, 76, 83]. This period is characterized by the development of an E-trending fault system strongly responsible for half-graben basin geometry associated with significant facies and thickness variations [76]. During Early Cretaceous times, the dominant N–S to NE-trending regional extension is associated with individualized sub-basins created due to the reactivation of

inherited fault systems. Besides, during this period, widespread salt tectonics are identified as being more active around the Tethyan domain and the Cretaceous tectogenesis is mainly influenced by the underlying Triassic salt strata [56, 96]. In the same way, in northern Tunisia, dozens of structures are documented as having grown during the Aptian–Albian period [32, 46, 63, 64, 75, 97]. Some structures were presented as dominated by raft tectonics on submarine salt bodies [63, 97]. Subsequently, numerous missing sequences in the El Kef area (e.g. Bled Doghra, Guern Halfaya and Nebeur area) are possibly the result of large raft tectonics especially active during Albian time, without implications of tertiary thrust systems.

The Cretaceous basin in northwest Tunisia reflects a basin's geometry very similar to the present-day Atlantic–type passive continental margins. This similarity can be seen in the existence of three mains units classically recognized in this context, i.e. pre-salt rifted basement, Triassic salt and post-salt (Jurassic–Cretaceous) sedimentary wedge. In Northern Tunisia, The syn-rift sediments that are up to 5 km are deposited in half-graben structures which seem to be dominant from Triassic to lower Cretaceous times (Fig. 13). This geometry is underlain by a series of major faults (probably listric) creating a basin with seaward facing submarine paleoslope hypothesized here to be ±5° northward. From within, the abundant intra-basin growth normal faults are responsible for a general northward motion such as raft tectonics. Commonly, from the tilted basement blocks to the intra-basin growth faults, the existence of Triassic evaporitic mobile rocks constitutes an excellent decoupling layer [68, 69, 56]. In brief, the northern Tunisia Cretaceous basin is predominantly a result of gravity deformation onto a general northward regional slope [63].

CONCLUSIONS

The Cretaceous basin in northern Tunisia is characterized by:

(1) Considerable sequences thickness variation due to repetitive depocenters geometry related to active normal major faults (probably listric) coupled by intra-basin growth faults.

(2) Abundant soft-sediment deformations.

(3) General N to NW-dipping submarine paleoslope hypothesized here to be ±5°, inferred here from slump folds analysis.

(4) Extensional tectonic regime which trends NNE to NE during Aptian-Albian, NW during Cenomanian, NNE to NE during Turonian-Coniacian and probably NW during Santonian.

All these features are fairly consistent with the conclusion that the structural style of this basin is very similar to the present-day Atlantic–type passive margins.

ACKNOWLEDGEMENTS

Authors are indebted to Prof. N. H. Woodcock (University of Cambridge, Cambridge, United Kingdom), Prof. I. G. Alsop (University of Aberdeen, Aberdeen, Scotland, United Kingdom) and Dr. L. J. Strachan (University of Auckland, Auckland, New Zealand) for great helpful discussions about the methodology, transport determination techniques and interpretation of slump folds. The Stereonet 9 software, written by R. Allmendinger (Cornell University, Ithaca, New York, United States) was used. We are grateful to Frank Thomas (Aix Marseille University, Marseille, France) for providing constructive help that substantially improved the structure of this paper.

Authors are grateful to anonymous Reviewer and reviewer Prof. Yu. L. Rebetsky (Shmidt Institute of Physics of the Earth, Moscow, Russia) for useful comments.

FINANCING

This work was financially supported by the Tunisian Ministry of Higher Education and Scientific Research (CERTE, Geo-resources Laboratory funding) and the French Ministry of Foreign Affairs grant through French Embassy in Tunisia (CMCU program).

REFERENCES

1. R. W. Allmendinger, N.C. Cardozo, and D. Fisher, *Structural geology algorithms: Vectors and tensors*, (Cambridge Univ. Press, Cambridge, UK, 2013), pp. 289.

2. G. I. Alsop, S. Marco, "Soft-sediment deformation within seismogenic slumps of the Dead Sea Basin," J. Struct. Geol. **33**, (4), 433–457 (2011).

3. G. I. Alsop, S. Marco, "A large-scale radial pattern of seismogenic slumping towards the Dead Sea basin," J. Geol. Soc. **169**, 1, 99–110 (2012a).

4. G. I. Alsop, S. Marco, "Tsunami and seiche-triggered deformation within offshore sediments," Sediment. Geol. **261–262**, 90–107 (2012b).

5. G. I. Alsop, S. Marco, "Seismogenic slump folds formed by gravity-driven tectonics down a negligible subaqueous slope," Tectonophysics, **605**, 48−69 (2013).

6. G. I. Alsop, S. Marco, "Fold and fabric relationships in temporally and spatially evolving slump systems: A multi-cell flow model," J. Struct. Geol. **63**, 27–49 (2014).

7. Z. Amri, C. Naji, A. Masrouhi, and O. Bellier, "Interconnection salt diapir–allochthonous salt sheet in northern Tunisia: The Lansarine–Baoula case study," J. Afr. Earth Sci. **170**, 103876 (2020).

8. J. Angelier, P. Mechler, "Sur une méthode graphique de recherche des contraintes principales également utilisable en tectonique et en séismologie: la méthode des dièdres droits," Bulletin de la société géologique de France. **19**, 1309–1318 (1977).

9. M. Bachari, D. Grosheny, S. Ferry, C. France-Lanord, and M. H. Negra, "The Cenomanian-Turonian boundary event (CTEB) in north-central Tunisia (Jebels Serj and

Bargou) integrated into regional data (Algeria to Tunisia),” Cretaceous Research. **94**, 108–125 (2018).

10. N. Bahrouni, Y. Houla, M. Soussi, M. Boughdiri, W. B. Ali, A. Nasri, and S. Bouaziz, “Discovery of Jurassic ammonite-bearing series in Jebel Bou Hedma (South-Central Tunisian Atlas): Implications for stratigraphic correlations and paleogeographic reconstruction,” J. Afr. Earth Sci. **113** (1), 101–113 (2016).

11. N. Bahrouni, F. Masson, F. Meghraoui, M. Saleh, R. Maamri, F. Dhaha, and M. Arfaoui, “Active tectonics and GPS data analysis of the Maghrebian thrust belt and Africa-Eurasia plate convergence in Tunisia,” Tectonophysics **785**, 228–440 (2020).

12. N. Ben Chaabane, F. Khemiri, M. Soussi, J.L. Latil, E. Robert, and I. Belhaj Taher, “Aptian-Lower Albian Serdj carbonate platform of the Tunisian Atlas: Development, demise and petroleum implication,” Marin. Petrol. Geol. **101**, 566–591 (2019).

13. A. Ben Ferjani, P. F. Burollet, and F. Mejri, *“Petroleum Geology of Tunisia,”* (ETAP Publ. 1990), pp.194.

14. *Geologic map of Tunisia 1:500.000*, Ed. by M. Ben Haj Ali, Y. Jedoui, T. Dali, H. Ben Salem, L. Memmi (Nation. Geol. Surv., Nation. Office of Mines, Tunisia, 1985).

15 S. Bey, J. Kuss, I. P. Silva, M. H. Negra, and S. Gardin, “Fault-controlled stratigraphy of Late Cretaceous Abiod formation at Ain Medheker (Northeast Tunisia),” Cretaceous Research, **34**, 10–25 (2012).

16. W. Bosworth, R. Guiraud, and L.G. Kessler, “Late Cretaceous (ca. 84 Ma) compressive deformation of the stable shelf of northeast Africa (Egypt); far-field stress effects of the “Santonian event” and origin of the Syrian arc,” Geology, **27**, 633–636 (1999).

17. M. H. P. Bott, “Rifted passive margins,” in *Developments in Geotectonics*, (Elsevier, 2006. Vol.25. Ch.11), pp. 409–426.

18. M. Boughdiri, F. Cordey, H. Sallouhi, K. Maalaoui, A. Masrouhi, and M. Soussi, “Jurassic radiolarian-bearing series of Tunisia: biostratigraphy and significance to western Tethys correlations,” Swiss J. Geosci. **100**, 431–441 (2007).

19. D. Bradley, L. Hanson, “Paleoslope Analysis of Slump Folds in the Devonian Flysch of Maine,” J. Geol. **106**, 305−318 (1998).

20. P. F. Burollet, “Contribution à l’étude stratigraphique de la Tunisie centrale,” Annales des mines et de la géologie, Tunisie, **18**, pp.345 (1956).

21. N. Cardozo, R. W. Allmendinger, “Spherical projections with OSX stereonet,” Comput. Geosci. **51**, 193–205 (2013).

22. T. Cavailhes, A. Rotevatn, S. Monstad, A. Ben Khala, E. Funk, K. Canner, M. Looser, A. Chalabi, A. Gay, A. Travé, F. Ferhi, A. Skanji, R. M. Chebbi, and N. Bang, “Basin tectonic history and paleophysiography of the pelagian platform, northern Tunisia, using vitrinite reflectance data,” Basin Research, **30**, 926–941 (2018).

23. M. Chikhaoui, A. L. Maamouri, J. Salaj, M. M. Turki, J. Saadi, M. Ben Youssef, M. Ghanmi, and M. Zarbout, “Tilted blocks during the Early Cretaceous in the El Kef area (northwestern Tunisia),” Comptes Rendus de l'Académie des Sciences - Series IIA – Earth Planet. Sci. **327**, 265–270 (1998).

24. T. N. Debacker, E. De Meester, “A regional, S-dipping late Early to Middle Ordovician palaeoslope in the Brabant Massif, as indicated by slump folds (Anglo-Brabant Deformation Belt, Belgium),” Geologica Belgica, **12**, 3-4, 145−159 (2009).

25. T. N. Debacker, “Folds and cleavage/fold relationships in the Brabant Massif, southeastern Anglo-Brabant Deformation Belt,” Geologica Belgica, **15**, 1-2, 81−95 (2012).

26. D. Delvaux, B. Sperner, “Stress tensor inversion from fault kinematic indicators and focal mechanism data: the TENSOR program,” Geol. Soc. London. Spec. Publ. **212**, 75–100 (2003).

27. C. Doglioni, E. Gueguen, F. Sabat, and M. Fernandez, “The western Mediterranean extensional basins and the Alpine orogeny,” Terra Nova **9**, 109–112 (1997).

28. C. G. Elliott, P. F. Williams, “Sediment slump structures: a review of diagnostic criteria and application to an example from Newfoundland,” J. Struct. Geol. **10**, 2, 171–182 (1988).

29. J. Frey-Martinez, J. Cartwrightn, and B. Hall, “3D seismic interpretation of slump complexes: examples from the continental margin of Israel,” Basin Research, **17**, 83–108 (2005).

30. D. Frizon de Lamotte, B. S. Bezar, R. Bracène, and E. Mercier,” The two main steps of the atlas building and geodynamics of the Western Mediterranean,” Tectonics, **19** (4), 740–761 (2002).

31. D. Frizon de Lamotte, C. Raulin, N. Mouchot, J. C. Wrobel-Daveau, C. Blanpied, and J. C. Ringenbach, “The southernmost margin of the Tethys realm during the Mesozoic and Cenozoic: Initial geometry and timing of the inversion processes,” Tectonics, **30** (3), TC3002 (2011).

32. M. Ghanmi, J. M. Vila, M. Ben Youssef, M. Jouirou, and F. Zargouni, “Diversité des Corps salifères du nord-est du Maghreb : Les lames et les lentilles triasiques de Touireuf à Nebeur (moyen Mellègue, nord-ouest tunisien) : Un « glacier de sel» sous-marin composite et

segmenté du Crétacé inférieur; intérêt pétrolier,'' in *Proceedings of the 10th Tunisian petroleum exploration & production conference*, (ETAP Mem. 2006. Vol.26) pp. 144–172.

33. M. Gharbi, A. Masrouhi, N. Espurt, O. Bellier, E. Amari, M. Ben Youssef, and M. Ghanmi, "New tectono-sedimentary evidences for Aptian to Santonian extension of the Cretaceous rifting in the Northern Chotts range (Southern Tunisia)," J. Afr. Earth Sci. **79**, 58–73 (2013).

34. M. Gharbi, O. Bellier, A. Masrouhi, and N. Espurt, "Recent spatial and temporal changes in the stress regime along the southern Tunisian Atlas front and the Gulf of Gabes: new insights from fault kinematics analysis and seismic profiles," Tectonophysics **626**, 120–136 (2014).

35. M. Gharbi, N. Espurt, A. Masrouhi, O. Bellier, and E. A. Amari, "Style of Atlassic tectonic deformation and geodynamic evolution of the southern Tethyan margin, Tunisia," Mar. Pet. Geol. **66**, 801–816 (2015).

36. *Geologic Map of Ouergha 1:50000, Sheet N°38*, Ed. by P. Sainfeld, J. Archambault, Des Ligneris, J. Pimenta, M. Arnould, (Nation. Geol. Surv., Nation. Office of Mines, Tunisia, 1951).

37. *Geologic Map of Le Kef 1:50000, Sheet N°44* Ed. by P. Sainfeld, P. F. Burollet, E. Dumon, (Nation. Geol. Surv., Nation. Office of Mines, Tunisia, 1953).

38. *Geologic Map of Maktar 1:50000, Sheet N°53* Ed. by A. Jauzein, A. Kouadja, G. Des Ligneris, D. Derthe, J. Quoix (Nation. Geol. Surv., Nation. Office of Mines, Tunisia, 1961).

39. *Geologic Map of Les Salines 1:50000, Sheet N°45* Ed. by K. Mahjoub (Nation. Geol. Surv., Nation. Office of Mines, Tunisia, 1992).

40. *Geologic Map of Nebeur 1:50000, Sheet N°39*, Ed. by M. Fakraoui, M. Ghanmi, M. Chikhaoui, A. Biely (Nation. Geol. Surv., Nation. Office of Mines, Tunisia, 1994).

41. *Geologic Map of Siliana 1:50000, Sheet N°46*, Ed. by M. Fakraoui, (Nation. Geol. Surv., Nation. Office of Mines, Tunisia, 1998).

42. *Geologic Map of Bargou 1:50000, Sheet N°47* Ed. by K. Mahjoub, T. Dali, (Nation. Geol. Surv., Nation. Office of Mines, Tunisia, 2000).

43. R. Guiraud, W. Bosworth, "Senonian basin inversion and rejuvenation of rifting in Africa and Arabia: synthesis and implications to plate-scale tectonics," Tectonophysics, **282**, 39–82 (1997).

44. R. Guiraud, "Mesozoic rifting and basin inversion along the northern African Tethyan margin: An overview," Geol. Soc. London, Spec. Publ. **133**, 217−229 (1998).

45. E. Jaillard, T. Dumont, J. Ouali, J. P. Bouillin, A. Chihaoui, J. L. Latil, H. Arnaud, H.A. Arnaud-Vanneau, and I. Zghal, " The Albian tectonic "crisis" in Central Tunisia: nature and chronology of the deformations," J. Afr. Earth Sci. **85**, 75–86 (2013).

46. E. Jaillard, J. P. Bouillin, J. Ouali, T. Dumont, J. L. Latil, and A. Chihaoui, "Albian salt tectonics in Central Tunisia: evidences for an Atlantic-type passive margin," J. Afr. Earth Sci. **135**, 220–234 (2017).

47. E. Jaillard, A. Chihaoui, J. L. Latil, and I. Zghal, "Sequences, discontinuities and water stratification in a low-energy ramp: the Early Albian sedimentation in central Tunisia," Int. J. Earth Sci. **110**, (1), 263–285 (2020).

48. C. Jallouli, S. Mogren, K. Mickus, and M. M. Turki, “Evidence for an east–west regional gravity trend in northern Tunisia: Insight into the structural evolution of northern Tunisian Atlas,” Tectonophysics **608**, 149–160 (2013).

49. O. T. Jones, “The geology of the Colwyn Bay district: a study of submarine slumping during the Salopian period,” Quarterly J. Geol. Soc. London **380**, 335–382 (1939).

50. O. T. Jones, “On the sliding or slumping of submarine sediments in Denbighshire, North Wales, during the Ludlow Period,” Quarterly J. Geol. Soc. London **93**, 241–283 (1940).

51. F. Kamoun, B. Peybernes, R. Ciszak, and S. Calzada, “Triassic paleogeography of Tunisia,” Palaeogeogr. Palaeoclimatol. Palaeoecol. **172**, (3-4), 223–242 (2001).

52. S. Khomsi, M. Bédir, M. Soussi, M. G. Ben Jemia, and K. Ben Ismail-Lattrache, “Mise en évidence en subsurface d’événements compressifs Eocène moyen-supérieur en Tunisie orientale (Sahel): Généralité de la phase atlasique en Afrique du Nord,” C. R. Géosci. **338** (1-2), 41–49 (2006).

53. S. Khomsi, M. G. Ben Jemia, D. Frizon de Lamotte, C. Maherssi, O. Echihi, and R. Mezni, “An overview of the Late Cretaceous-Eocene positive inversions and Oligo-Miocene subsidence events in the foreland of the Tunisian Atlas: structural style and implications for the tectonic agenda of the Maghrebian Atlas system,” Tectonophysics **475**, 38–58 (2009).

54. S. Khomsi, D. F. de Lamotte, M. Bédir, and O. Echihi, “The Late Eocene and Late Miocene fronts of the Atlas Belt in eastern Maghreb: Integration in the geodynamic evolution of the Mediterranean Domain,” Arab. J. Geosci. **9**, 650, 1-20 (2016).

55. S. Khomsi, F. Roure, M. Khelil, R. Mezni, and O. Echihi, “A review of the crustal architecture and related pre-salt oil/gas objectives of the eastern Maghreb Atlas and Tell: Need for deep seismic reflection profiling,” Tectonophysics **766**, 232–248 (2019).

56. *Geological Framework of the Levant. Volume 1: Cyprus and Syria*, Ed. by V. A. Krasheninnikov, J. K. Hall, F. Hirsch, H. Benjamini, A. Flexer (Historical Productions-Hall, Jerusalem, Israel, 2005).

57. R. Leprêtre, D. Frizon de Lamotte, V. Combier, O. Gimeno-Vives, G. Mohn, and R. Eschard, "The Tell-Rif orogenic system (Morocco, Algeria, Tunisia) and the structural heritage of the southern Tethys margin," BSGF - Earth Sci. Bull. **189** (2), 1-10 (2018).

58. C. Martinez, M. Chikhaoui, R. Truillet, J. Ouali, and G. Creuzot, "Le contexte géodynamique de la distension albo-aptienne en Tunisie septentrionale et centrale: structuration éocrétacée de l'Atlas tunisien," Eclogae geologicae Helvetiae, **84** (1), 61–82 (1991).

59. J. D. Martín-Martín, J. Vergés, E. Saura, M. Moragas, G. Messager, V. Baqués, P. Razin, C. Grélaud, M. Malaval, R. Joussiaume, E. Casciello, I. Cruz-Orosa, and D. W. Hunt, "Diapiric growth within an Early Jurassic rift basin: the Tazoult salt wall (Central High Atlas, Morocco): Diapiric growth of the Tazoult salt wall," Tectonics **36** (1), 2–32 (2017).

60. A. Masrouhi, M. Ghanmi, M. M. Ben Slama, M. Ben Youssef, J. M. Vila, F. Zargouni, "New tectono-sedimentary evidence constraining the timing of the positive tectonic inversion and the Eocene Atlasic phase in northern Tunisia: implication for the North African paleo-margin evolution," Comptes Rendus Geosci. **340**, 771–778 (2008).

61. A. Masrouhi, H. A. Koyi, "Submarine 'salt glacier' of Northern Tunisia, a case of Triassic salt mobility in North African Cretaceous passive margin," Geol. Soc. London, Spec. Publ. **363**, 579–593 (2012).

62. A. Masrouhi, O. Bellier, H. Koyi, J. M. Vila, M. Ghanmi, “The evolution of the Lansarine–Baouala salt canopy in the North African Cretaceous passive margin in Tunisia,” Geol. Magazine, **150** (5), 835–861 (2013).

63. A. Masrouhi, O. Bellier, M. Ben Youssef, and H. Koyi, “Submarine allochthonous salt sheets: gravity-driven deformation of North African Cretaceous passive margin in Tunisia – Bled Dogra case study and nearby salt structures,” J. Afr. Earth Sci. **97**, 125–142 (2014a).

64. A. Masrouhi, O. Bellier, and H. Koyi, “Geometry and structural evolution of Lorbeus diapir, northwestern Tunisia: polyphase diapirism of the North African inverted passive margin,” Int. J. Earth Sci. (Geol. Rundsch.) **103**, 881–900 (2014b).

65. A. Masrouhi, M. Gharbi, O. Bellier, and M. Ben Youssef, “The Southern Atlas Front in Tunisia and its foreland basin: Structural style and regional-scale deformation,” Tectonophysics **764**, 1–24 (2019).

66. H. Mattoussi Kort, D. Gasquet, M. Ikenne, and N. Laridhi Ouazaa, “Cretaceous crustal thinning in North Africa: implications for magmatic and thermal events in the Eastern Tunisian margin and the Pelagic Sea,” J. Afr. Earth Sci. **55**, (5), 257–264 (2009).

67. L. Memmi, “L'Aptien et l'Albien de Tunisie : biostratigraphie à partir des ammonites,” Bulletin de la Société Géologique de France **170** (3), 303–309 (1999).

68. M. Moragas, J. Vergés, E. Saura, J. D. Martín-Martín, G. Messager, O. Merino Tomé, I. Suarez-Ruiz, P. Razin, C. Grélaud, M. Malaval, R. Joussiaume, and D. W. Hunt, “Jurassic rifting to post-rift subsidence analysis in the Central High Atlas and its relation to salt diapirism,” Basin Research **30**, 336–362 (2016).

69. M. Moragas, J. Vergés, T. Nalpas, E. Saura, J. D. Martin-Martin, G. Messager, and D. W. Hunt, “The impact of syn- and post-extension prograding sedimentation on the development

of salt-related rift basins and their inversion: Clues from analogue modeling," Marin. Petrol. Geol. **88**, 985–1003 (2017).

70. M. Moragas, V. Baqués, A. Travé, J. D. Martín-Martín, E. Saura, G. Messager, D. W. Hunt, and J. Vergés, "Diagenetic evolution of lower Jurassic platform carbonates flanking the Tazoult salt wall (Central High Atlas, Morocco)," Basin Research **32** (3), 546–566 (2019).

71. C. Morelli, R. Nicolich, "A cross section of the lithosphere along the European Geotraverse Southern Segment (from the Alps to Tunisia)," Tectonophysics **176** (1-2), 229–243 (1990).

72. C. Naji, M. Gharbi, Z. Amri, A. Masrouhi, and O. Bellier,"Temporal and spatial changes of the submarine Cretaceous paleoslope in Northern Tunisia, inferred from Slump folds analysis," Proceeding of the Geologists Association, **129**, 40–56 (2018a).

73. C. Naji, A. Masrouhi, Z. Amri, M. Gharbi, and O. Bellier,"Cretaceous paleomargin tilted blocks geometry in northern Tunisia: stratigraphic consideration and fault kinematic analysis," Arab. J. Geosci. **11**, (583), 1–21 (2018b).

74. H. Ortner, "Styles of soft-sediment deformation on top of a growing fold system in the Gosau Group at Muttekopf, Northern Calcareous Alps, Austria: Slumping versus tectonic deformation," Sediment. Geol. **196**, (1-4), 99–118 (2007).

75. V. Perthuisot, H. Rouvier, and A. Smati, "Style et importance des déformations anté-vraconnienes dans le Maghreb oriental: exemple du diapir du Jebel Slata," Bulletin de la Société Géologique de France **8**, 389–398 (1998).

76. C. Raulin, D. F. de Lamotte, S. Bouaziz, S. Khomsi, N. Mouchot, G. Ruiz, and F. Guillocheau, "Late Triassic–early Jurassic block tilting along E–W faults, in southern

Tunisia: New interpretation of the Tebaga of Medenine," J. Afr. Earth Sci. **61** (1), 94–104 (2011).

77. Yu.L. Rebetsky, N. A. Sycheva, O. A. Kuchay, and R. E. Tatevossian, "Development of inversion methods on fault slip data. Stress state in orogenes of the central Asia," Tectonophysics, **581**, 114-131 (2012).

78. Yu.L. Rebetsky, L. A. Sim, and A. V. Marinin, "From sliding mirrors to tectonic stresses. Methods and algorithms," M.: GEOS. (In Russian), 234 p (2017).

79. Yu. L. Rebetsky and A. Yu. Polets, "The method of cataclastic analysis of discontinuous displacements," in. *Moment Tensor Solutions*, Ed. by Sebastiano D'Amico (Springer Natural Hazards, 2018), pp. 111-162.

80. Research Group for Lithospheric Structure in Tunisia, "The EGT'85 seismic experiment in Tunisia: A reconnaissance of the deep structures," Tectonophysics, **207**, 245–267 (1992).

81. F. Robaszynski, F. Amédro, and M. Caron, "La limite Cénomanien-Turonien et la Formation Bahloul dans quelques localités de Tunisie Centrale," Cretaceous Research **14**, 4–5, 477–486 (1993).

82. F. Robaszynski, "The upper cretaceous of the kalaat Senan region, central Tunisia. Integrated litho-biostratigraphy based on ammonites, planktonic foraminifera and nannofossils zones from upper Turonian to Maastrichtian," Bulletin des Centres de Recherches (Elf Explor. Product.) **22**, 2, 359–490 (2000).

83. E. Saura, J. Vergés, J. D. Martín-Martín, G. Messager, M. Moragas, P. Razin, C. Grélaud, R. Joussiaume, M. Malaval, S. Homke, and D. W. Hunt, "Syn- to post-rift diapirism and minibasins of the Central High Atlas (Morocco): the changing face of a mountain belt," J. Geol. Soc., London **171**, 97–105 (2014).

84. A. W. Snoke, S. Schamel, and R. M. Karasek, “Structural evolution of Djebel Debadib anticline: A clue to the regional tectonic style of the Tunisian Atlas,” Tectonics **7** (3), 497–516 (1988).

85. M. Soua, N. Tribovillard, “Modèle de sédimentation au passage Cénomanien/Turonien pour la formation Bahloul en Tunisie,” Cretaceous Research **339**, 692–701 (2007).

86. M. Soua, O. Echihi, M. Herkat, D. Zaghbib-Turki, J. Smaoui, H. Fakhfakh-Ben Jemia, and H. Belghaji, “Structural context of the paleogeography of the Cenomanian–Turonian anoxic event in the eastern Atlas basins of the Maghreb,” Cretaceous Research **341**, 1029–1037 (2009).

87. P. Souquet, B. Peybernes, J. Saadi, M. Ben Youssef, M. Ghanmi, M. Zarbout, M. Chikhaoui, and F. Kamoun, “Séquences et cycles d’ordre 2 en régime extensif et transtensif: exemple du Crétacé inférieur de l’Atlas tunisien,” Bulletin de la Société géologique de France **168**, 373–386 (1997).

88. M. Soussi, G. Niedźwiedzki, M. Tałanda, D. Dróżdż, T. Sulej, K. Boukhalfa, J. Mermer, B. Błażejowski, “Middle Triassic (Anisian-Ladinian) Tejra red beds and Late Triassic (Carnian) carbonate sedimentary records of southern Tunisia Saharan Platform: Biostratigraphy, sedimentology and implication on regional stratigraphic correlations,” Marin. Petrol. Geol. **79**, 222–256 (2017).

89. L. J. Strachan, G. I. Alsop, “Slump folds as estimators of palaeoslope: a case study from the Fisherstreet Slump of County Clare, Ireland,” Basin Research **18**, 451–470 (2006).

90. L. J. Strachan, “Flow transformations in slumps: a case study from the Waitemata Basin, New Zealand,” Sedimentology **55**, 1311−1332 (2008).

91. M. D. Tranos, “The use of Stress Tensor Discriminator Faults in separating heterogeneous fault-slip data with best-fit stress inversion methods,” J. Struct. Geol. **102**, 168–178 (2017).

92. *Polycinématique et contrôle sédimentaire associée sur la cicatrice Zaghouan-Nebhana*, Ed. by M. M. Turki, (Thèse Doctorat d’Etat, Université de Tunis et Revue Sciences de la Terre, Tunisie. 1985. Vol.7), pp.228.

93. *Etude géologique du Massif Serj-Bargou (Atlas tunisien central)*, Ed. by M. M. Turki, (Thèse 3ème cycle, Université Pierre Et Marie Curie Paris. 1975. Vol.5), pp.85.

94. M. M. Turki, “Les inversions tectoniques de la Tunisie centro-septentrionale, ” Bulletin de la Société Géologique de France **8** (3), 399–406 (1988).

95. A. J. Van Loon, “Soft-sediment deformation structures in siliciclastic sediments: An overview,” Geologos **15** (1), 3–55 (2009).

96. J. Vergés, Y. Poprawski, Y. Almar, P. A. Drzewiecki, M. Moragas, T. Bover-Arnal, C. Macchiavelli, W. Wright, G. Messager, J. C. Embry, and D. Hunt, “Tectono-sedimentary evolution of Jurassic–Cretaceous diapiric structures: Miravete anticline, Maestrat Basin, Spain,” Basin Research **32**, (6), 1653–1684 (2020).

97. J. M. Vila, M. Ben Youssef, S. Bouhlel, M. Ghanmi, S. Kassâa, and F. Miaadi, “Tectonique en radeaux au toit d'un ‘‘glacier de sel’’ sous-marin albien de Tunisie du Nord-Ouest: Exemple du secteur minier de Gueurn Halfaya,” Comptes Rendus de l'Académie des Sciences **327**, 563–570 (1998).

98. N. H. Woodcock, “Ludlow Series slumps and turbidites and the form of the Montgomery Trough, Powys, Wales,” Proc. Geol. Assoc. **87**, 169–182 (1976a).

99. N. H. Woodcock, “Structural style in slump sheets: Ludlow series Powys, Wales,” J. Geol. Soc., London **132**, 399–415 (1976b).

100. N. H. Woodcock, “The use of slump structures as palaeoslope orientation estimators,” Sedimentology **26**, 83−99 (1979).

FIGURE CAPTIONS for N.Chahreddine and co-authors

Fig. 1. Tectonic map of northern Tunisian Atlas system with the geological map of the study area (after [14], modified).

The inset on the top left (a) shows the location of Tunisia in North Africa.

Blue rectangles into the inset (b) indicate the boundaries of the 1:50000 geological maps in northwestern Tunisia subject of this study, with: 38: Ouergha [36]; 39: Nebeur [40]; 44: Le Kef [37]; 45: Les Salines [39]; 53: Makthar [38]; 46: Siliana [41]; 47: Jebel Bargou [42] and 54) Jebel Serj geologic map areas.

Fig. 2. Lithostratigraphic correlation of Late Cretaceous series of El kef–Siliana area.

The inset in the midst shows the location of measured sections.

Fig. 3. Fold's patterns in slumping sheet.

(a) Model used to relate slump fold geometry to paleoslope attitude (after [99]);

(b) Fold facing direction in schematic illustrations summarizing the relationships between folds vergence, axial plane and up-ward or downward facing states (after [3]);

(c) Equal area plot of hypothetical fold axis and poles of axial planes distribution to illustrate the mean axis, the separation, and the axial plane methods. The best fit girdle to axes and poles to axial planes of the slump sheet are horizontals. The paleoslope dips to south (after [100]).

Fig. 4. Field photos of normal faults.

(a) Sealed normal faults, with growth strata geometry, Cenomanian–Early Turonian. The inset in the bottom right illustrates an olistolith structure.

(b) Abundant small-scale normal faults, sometimes with tilted-block geometry–Cenomanian associated to soft-sediment deformations (slump folds and olistoliths blocks)

Fig. 5. Field photos illustrating the Coniacian–Santonian faulting.

(a)–(b) Sealed normal faults affected the Coniacian sequences of Zaafrana section.

(c)–(d) well preserved meso-scale synsedimentary normal faults collected from Coniacian-Santonian sequences of the southern limb of Serj-Ballouta structure.

(e) Synsedimentary sealed normal fault collected from Santonian series of the southern limb of Serj-Ballouta structure.

Fig. 6. Geologic map of Jebel Ballouta, Jebel Serj and Jebel Bargou (after [9, 42], modified) with the back-tilted stress tensors diagrams of fault populations collected from this area.

Stress axis: maximum σ1 (circle); intermediate σ2 (triangle); minimum σ3 (square).

Fig. 7. Geologic map of Zaafrana area (after [14], modified) with the back-tilted stress tensors diagrams of Coniacian–Santonian fault populations collected from this region.

Stress axis: maximum σ1 (circle); intermediate σ2 (triangle); minimum σ3 (square).

Fig. 8. Lower hemisphere projection of back-tilted major fault data sets showing the regional paleostress regime in northwestern Tunisia during Late Cretaceous.

Fig. 9. Slump folding data and paleoslope reconstruction in Jebel Sidi-Amor and Jebel Bargou.

(1) Valanginian–Hauterivian paleoslope orientation of Jebel Sidi-Amor area with;

(a) Equal area projection of back-tilted slump axis (red box) and poles to axial planes (blue triangles) with respectively MAM (red arrow) and APM (blue arrow) methods.

(b)–(c) Field photos showing well preserved slump folds.

(2) Albian paleoslope orientation of Jebel Bargou structure with;

(a) Field photo illustrating preserved slump fold structure.

(b) Equal area projection of back-tilted slump axis (red box) and poles to axial planes (blue triangles) with respectively MAM (red arrow) and APM (blue arrow) methods.

Fig. 10. Cenomanian slump folding data and paleoslope reconstruction in Jebel Serj.

(a) Field photos showing well preserved slump folds in the nodular Cenomanian strata.

(b) Equal area projection of back-tilted slump axis (red box) and poles to axial planes (blue triangles) with respectively MAM (red arrow) and APM (blue arrow) methods.

Fig. 11. Slump folding data and paleoslope reconstruction in Zaafrana and Bled Doghra during Conician–Santonian:

(1) Paleoslope orientation in Zaafrana area with;

(a)–(b) Field photos showing well preserved slump folds.

(c) Equal area projection of back-tilted slump axis (red box) and poles to axial planes (blue triangles) with respectively MAM (red arrow) and APM (blue arrow) methods.

(2) Paleoslope orientation in Bled Doghra area with;

(a) Field photo showing preserved slump structure.

(b) Equal area projection of back-tilted slump axis (red box) and poles to axial planes (blue triangles) with respectively MAM (red arrow) and APM (blue arrow) methods.

Fig. 12. Slump folding data and paleoslope reconstruction in Jebel Serj-Ballouta and Jebel Lorbeus during Coniacian–Santonian.

(1) Paleoslope orientation in Jebel Serj-Ballouta area with:

(a) Equal area projection of back-tilted slump axis (red box) and poles to axial planes (Blue triangles) with respectively MAM (red arrow) and APM (blue arrow) methods.

(b)–(d) Field photos showing well preserved Coniacian–Santonian slump folds.

(2) Paleoslope orientation in Jebel Lorbeus area with:

(a) Equal area projection of back-tilted slump axis (red box) and poles to axial planes (Blue triangles) with respectively MAM (red arrow) and APM (blue arrow) methods.

(b) Field photo showing well preserved Coniacian–Santonian slumping sheet.

Fig.13. Schematic cross section of northwestern Tunisia domain during Cretaceous showing the structural configuration of the basin with widespread soft-sediment deformation onto north-facing submarine paleoslope related to the Tethyan margin expansion.

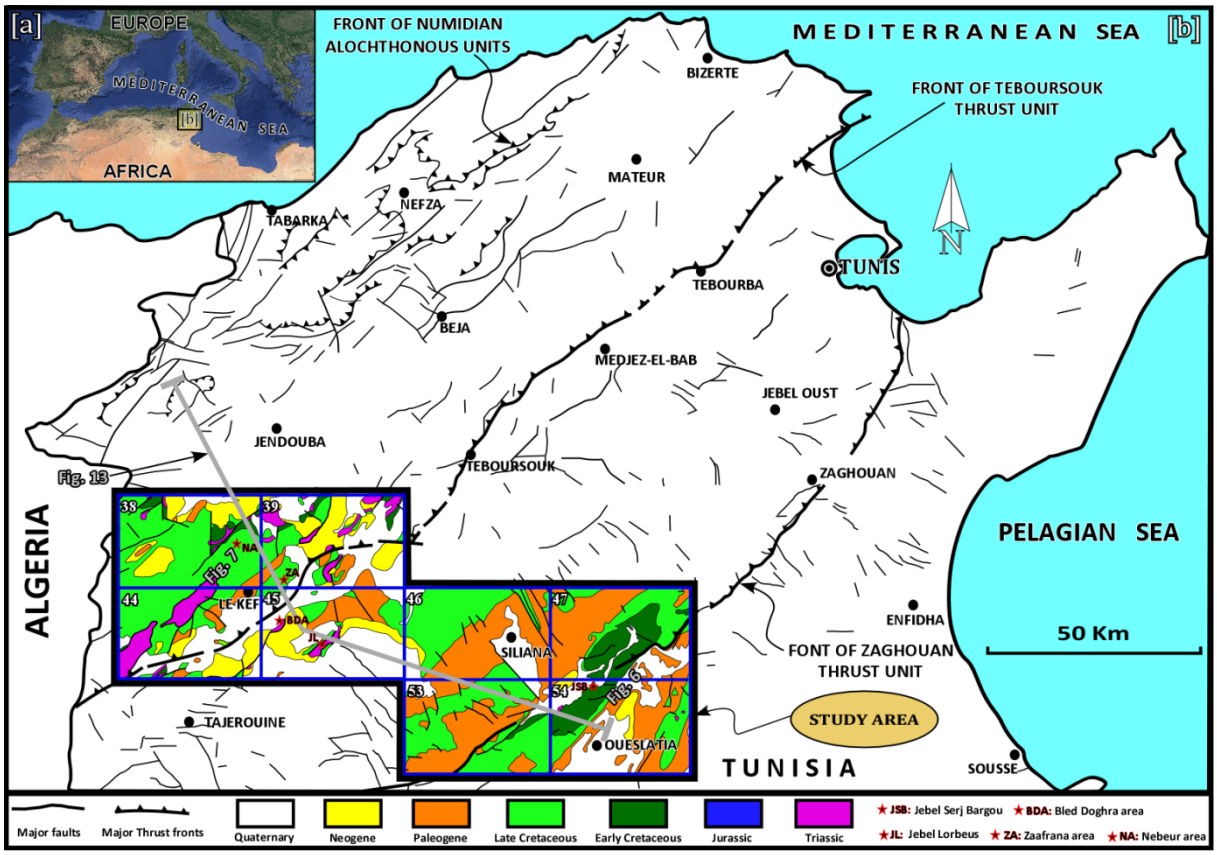


Fig.1 (modified)

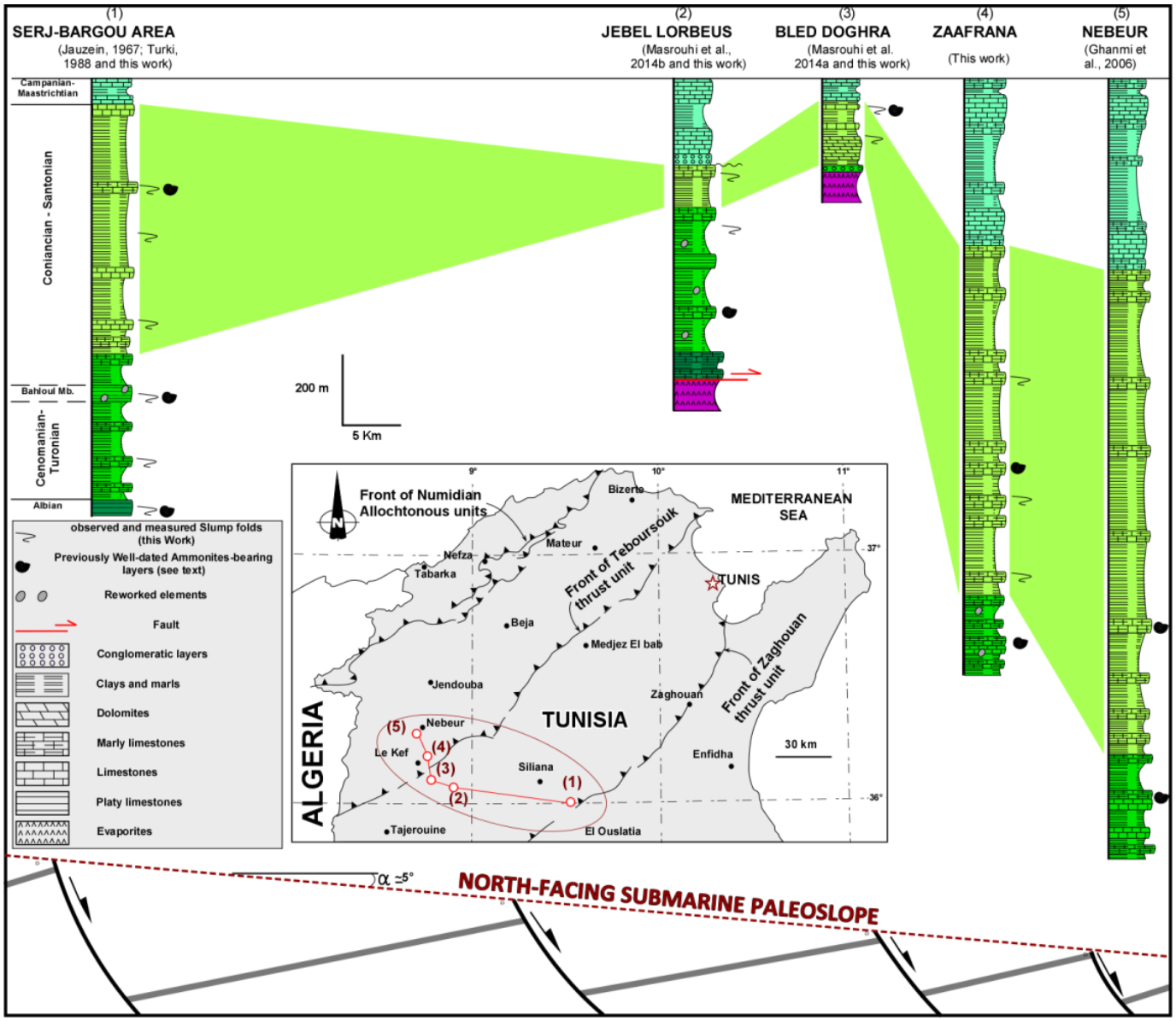

(1)
SERJ-BARGOU AREA
(Jauzein, 1967; Turki, 1988 and this work)
(2)
JEBEL LORBEUS
(Masrouhi et al., 2014b and this work)
(3)
BLED DOGHRA
(Masrouhi et al. 2014a and this work)
(4)
ZAAFRANA
(This work)
(5)
NEBEUR
(Ghanmi et al., 2006)
Campanian-Maastrichtian
Coniancian - Santonian
Bahloul Mb.
Cenomanian-Turonian
Albian
200 m
5 Km
observed and measured Slump folds (this Work)
Previously Well-dated Ammonites-bearing layers (see text)
Reworked elements
Fault
Conglomeratic layers
Clays and marls
Dolomites
Marly limestones
Limestones
Platy limestones
Evaporites
Front of Numidian Allochtonous units
MEDITERRANEAN SEA
Bizerte
Mateur
Nefza
Tabarka
Front of Teboursouk thrust unit
TUNIS
Beja
Medjez El bab
Jendouba
Zaghouan
Front of Zaghouan thrust unit
ALGERIA
TUNISIA
Nebeur
Le Kef
Siliana
Enfidha
30 km
Tajerouine
El Ouslatia
9°
10°
11°
37°
36°
α ≈5°
NORTH-FACING SUBMARINE PALEOSLOPE

Fig.2

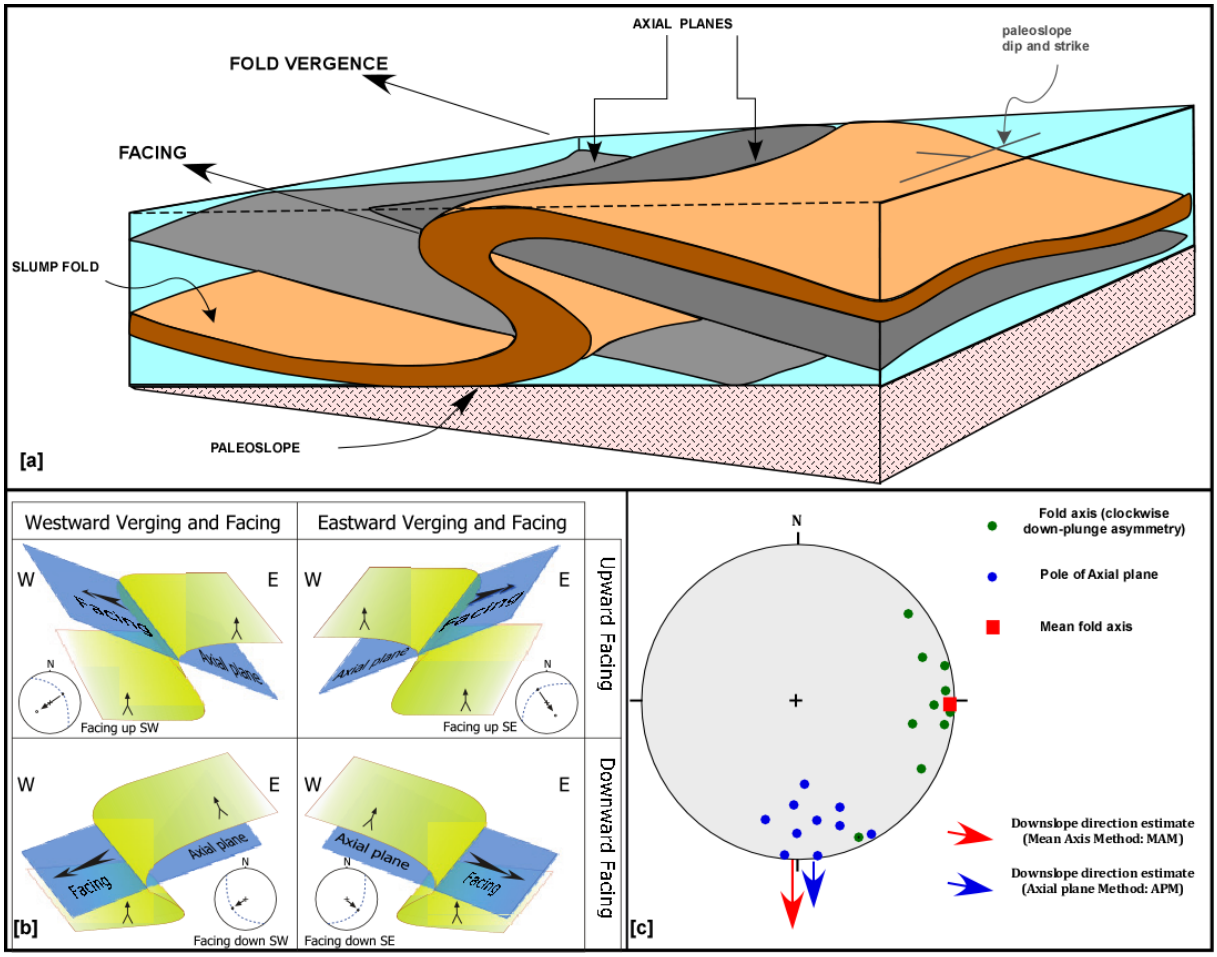


Fig.3 (modified)

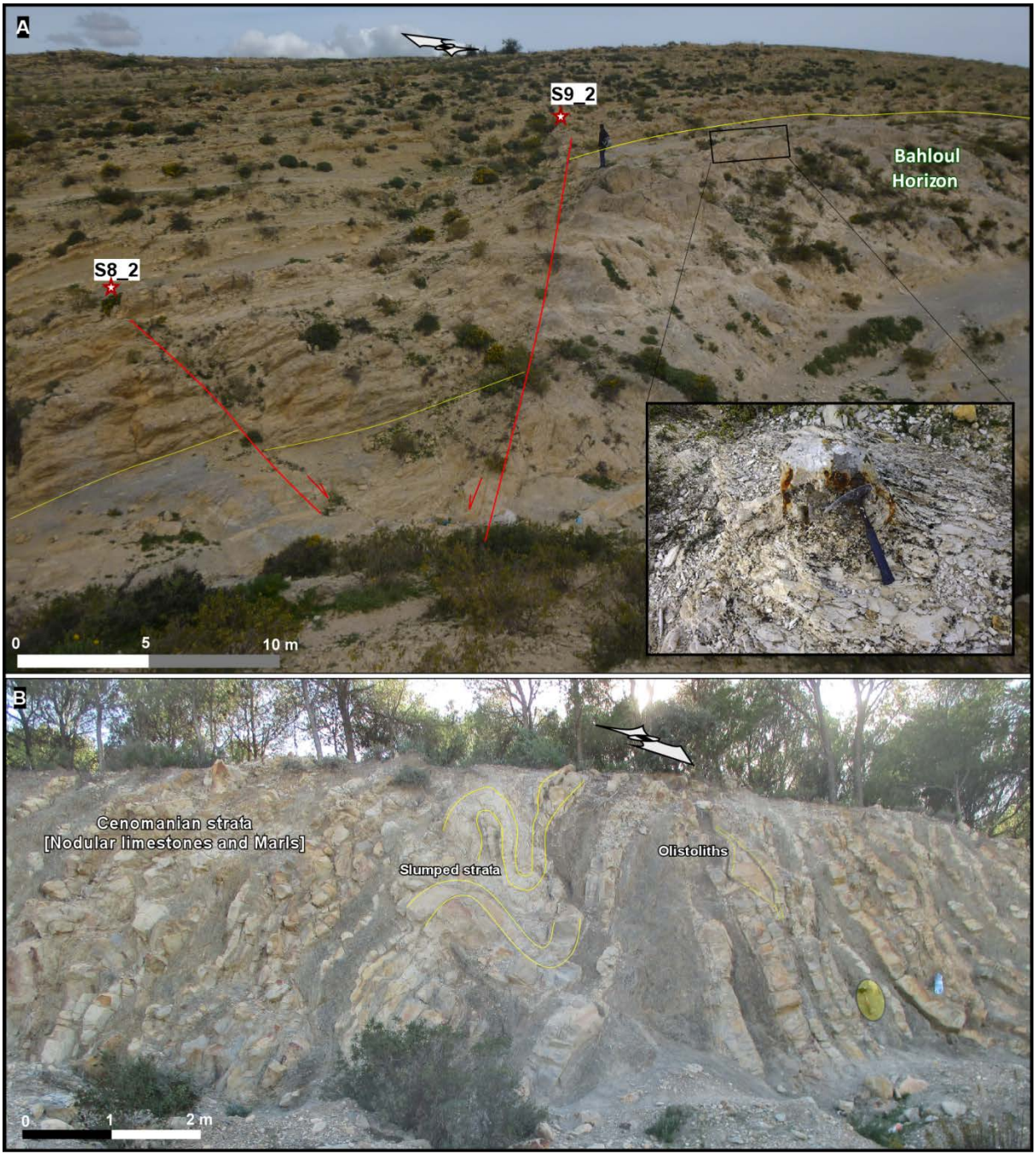

A
S9_2
S8_2
Bahloul
Horizon
0
5
10 m
B
Cenomanian strata
[Nodular limestones and Marls]
Slumped strata
Olistoliths
0
1
2 m

Fig.4

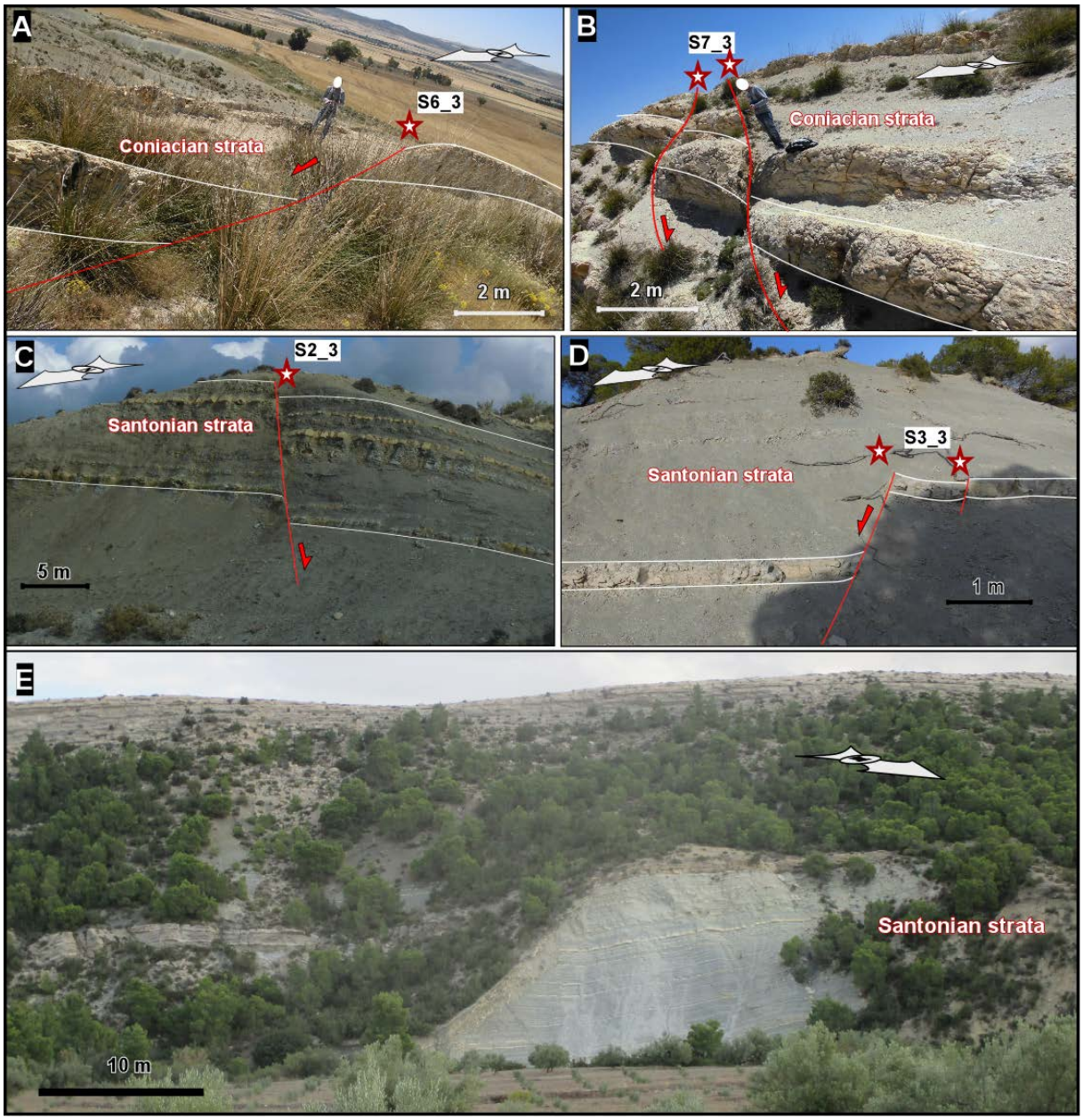

A
S6_3
Coniacian strata
2 m
B
S7_3
Coniacian strata
2 m
C
S2_3
Santonian strata
5 m
D
S3_3
Santonian strata
1 m
E
Santonian strata
10 m

Fig.5

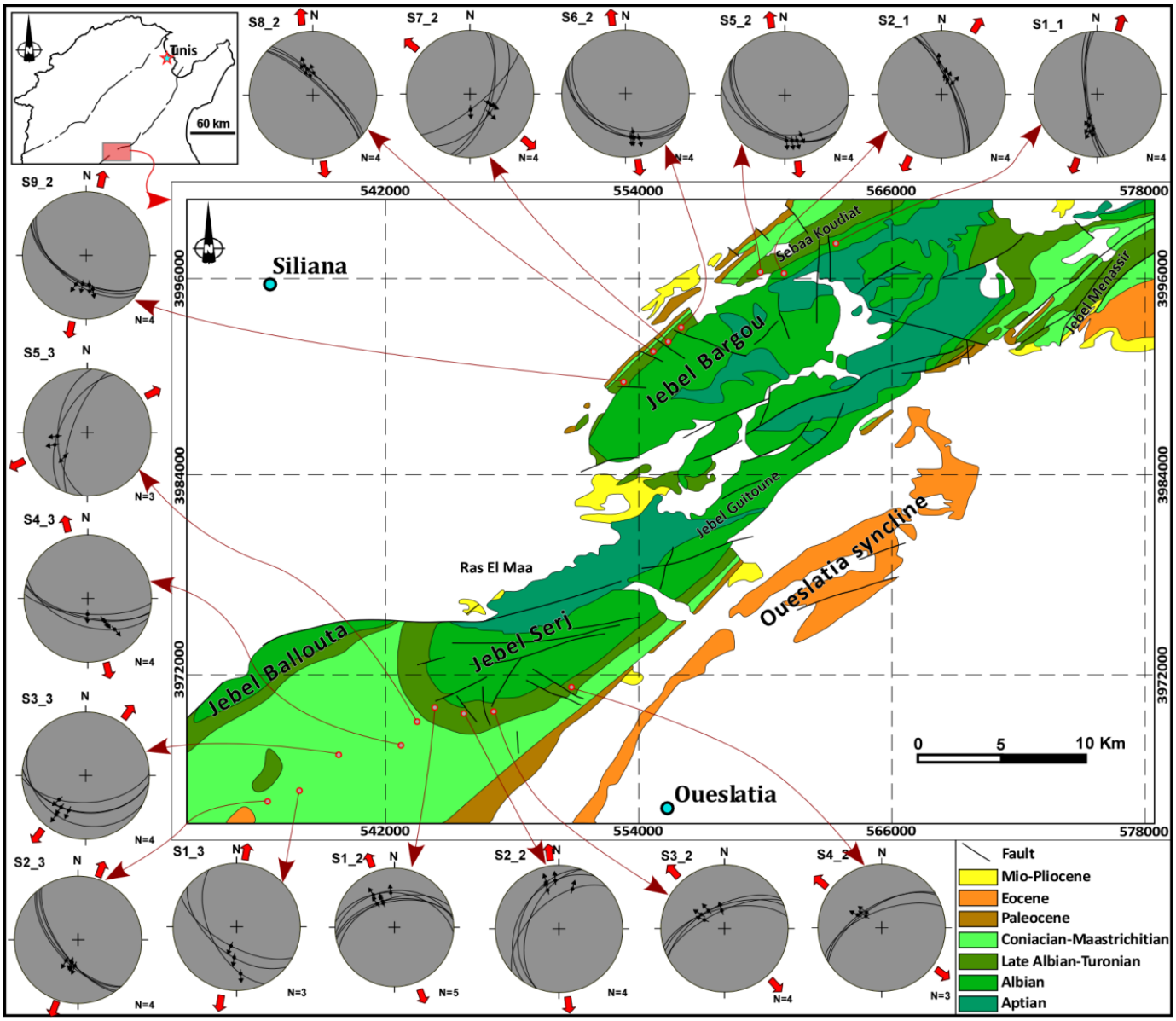

Tunis
60 km
S8_2
S7_2
S6_2
S5_2
S2_1
S1_1
S9_2
S5_3
S4_3
S3_3
S2_3
S1_3
S1_2
S2_2
S3_2
S4_2
N=4
N=3
N=5
542000
554000
566000
578000
3996000
3984000
3972000
Siliana
Sebaa Koudiat
Jebel Bargou
Jebel Menassir
Jebel Guitoune
Ras El Maa
Oueslatia syncline
Jebel Ballouta
Jebel Serj
Oueslatia
0
5
10 Km
Fault
Mio-Pliocene
Eocene
Paleocene
Coniacian-Maastrichitian
Late Albian-Turonian
Albian
Aptian

Fig.6

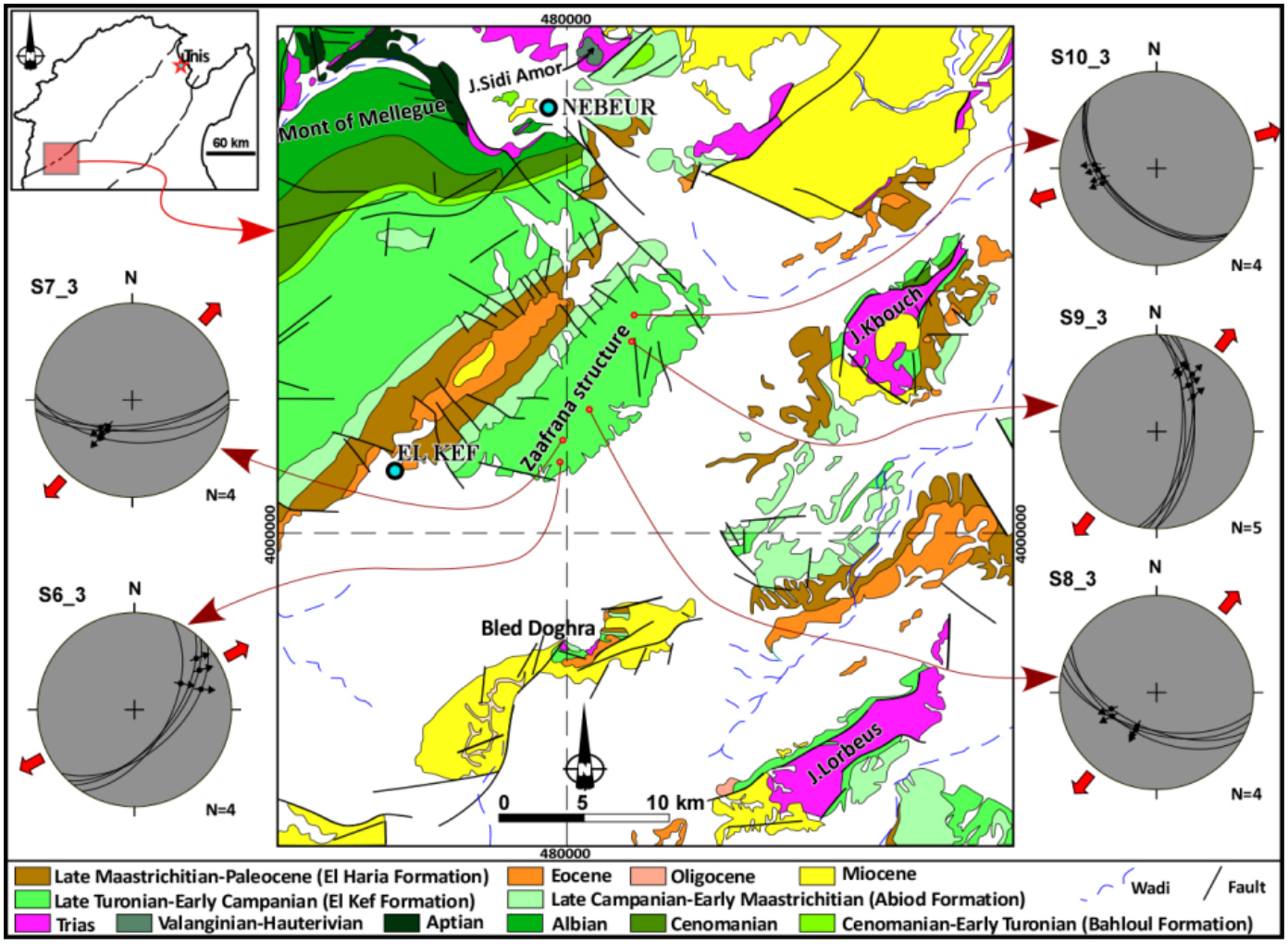

Tunis
60 km
480000
J.Sidi Amor
NEBEUR
Mont of Mellegue
EL KEF
Zaafrana structure
J.Kbouch
Bled Doghra
J.Lorbeus
4000000
0
5
10 km
S10_3
N
N=4
S9_3
N=5
S8_3
N=4
S7_3
N=4
S6_3
N=4
Late Maastrichitian-Paleocene (El Haria Formation)
Eocene
Oligocene
Miocene
Late Turonian-Early Campanian (El Kef Formation)
Late Campanian-Early Maastrichitian (Abiod Formation)
Trias
Valanginian-Hauterivian
Aptian
Albian
Cenomanian
Cenomanian-Early Turonian (Bahloul Formation)
Wadi
Fault

Fig.7

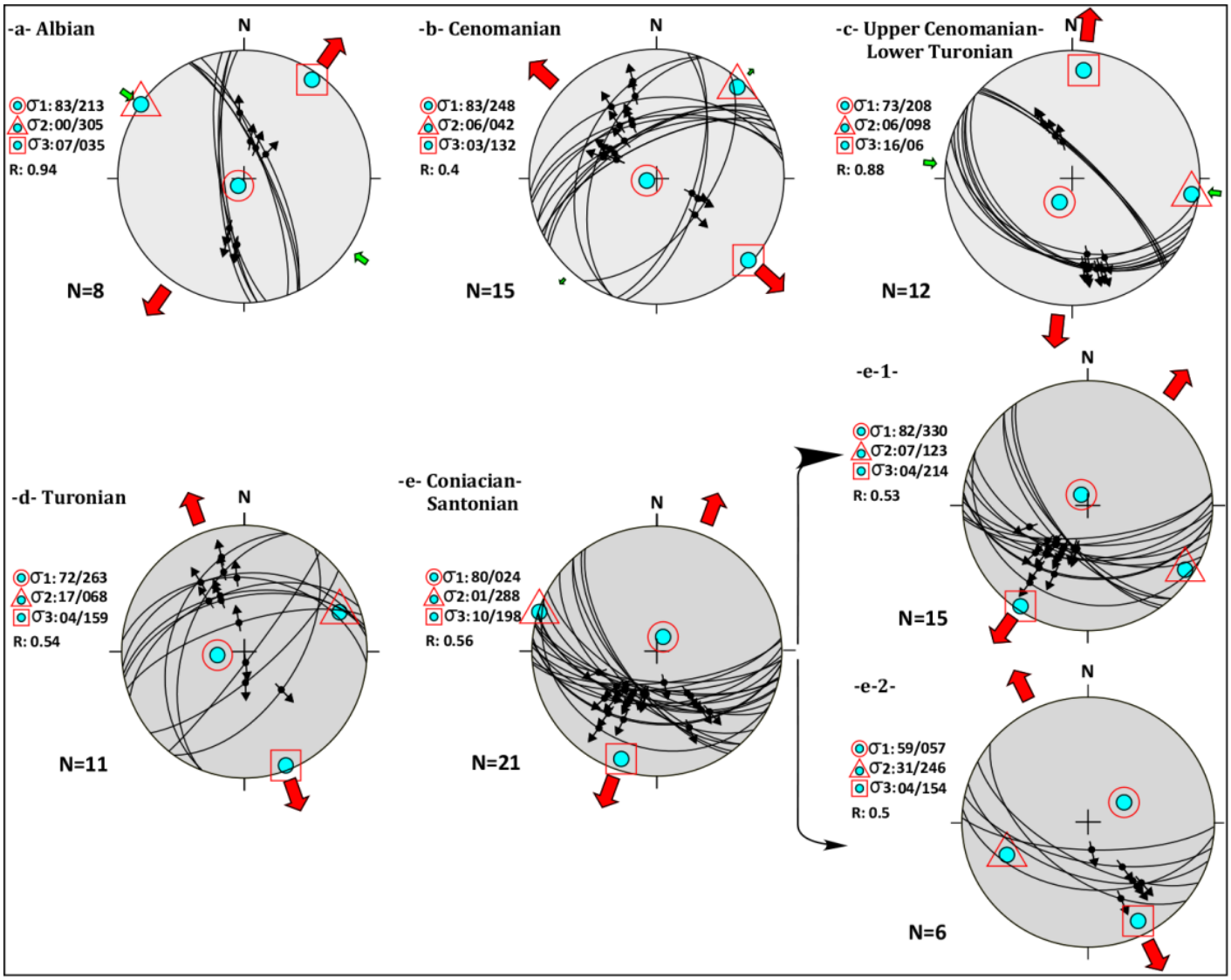

-a- Albian
σ1: 83/213
σ2: 00/305
σ3: 07/035
R: 0.94
N=8
-b- Cenomanian
σ1: 83/248
σ2: 06/042
σ3: 03/132
R: 0.4
N=15
-c- Upper Cenomanian-
Lower Turonian
σ1: 73/208
σ2: 06/098
σ3: 16/06
R: 0.88
N=12
-d- Turonian
σ1: 72/263
σ2: 17/068
σ3: 04/159
R: 0.54
N=11
-e- Coniacian-
Santonian
σ1: 80/024
σ2: 01/288
σ3: 10/198
R: 0.56
N=21
-e-1-
σ1: 82/330
σ2: 07/123
σ3: 04/214
R: 0.53
N=15
-e-2-
σ1: 59/057
σ2: 31/246
σ3: 04/154
R: 0.5
N=6

Fig.8

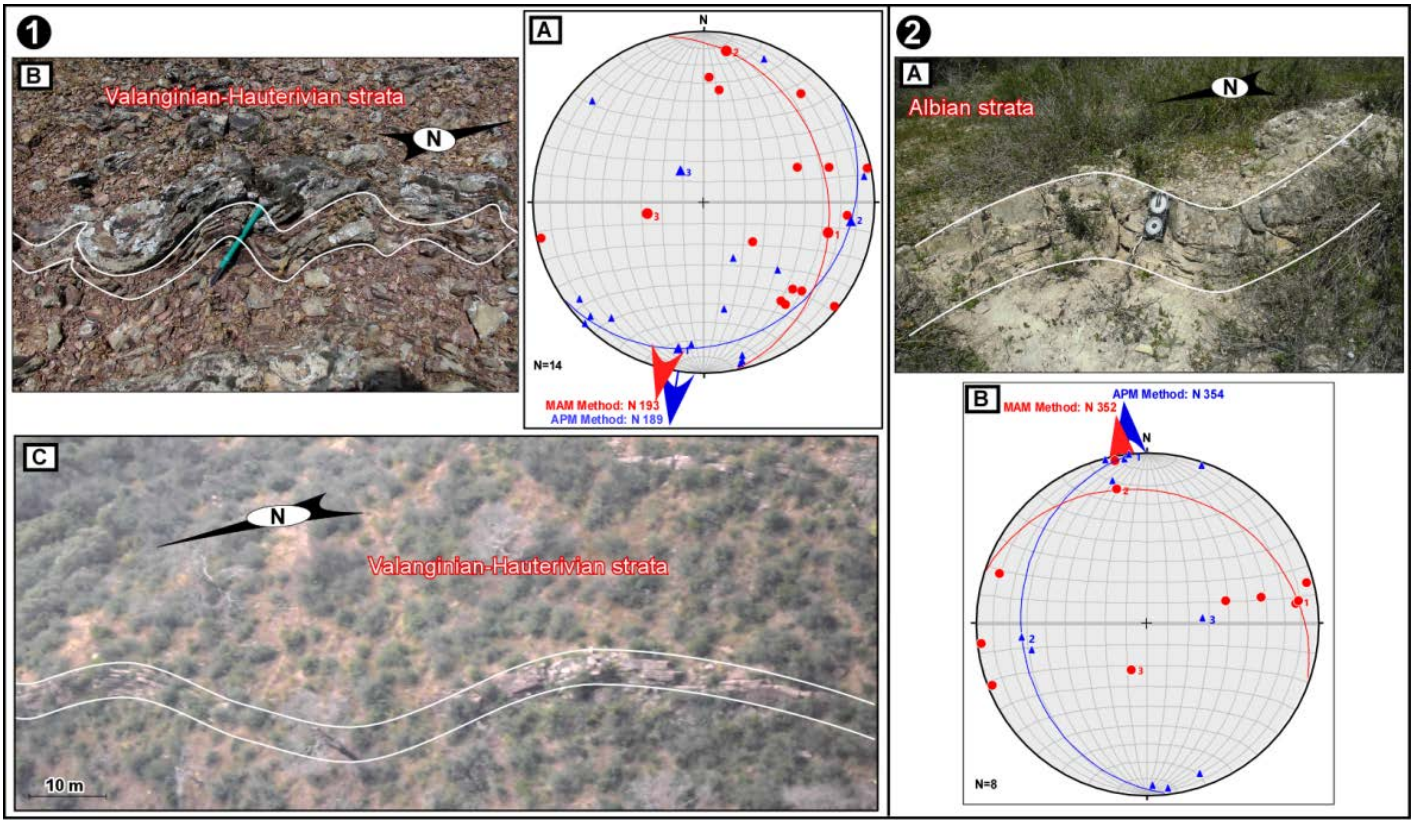

1
B
Valanginian-Hauterivian strata
N
A
N
N=14
MAM Method: N 193
APM Method: N 189
C
N
Valanginian-Hauterivian strata
10 m
2
A
Albian strata
N
B
APM Method: N 354
MAM Method: N 352
N
N=8

Fig.9

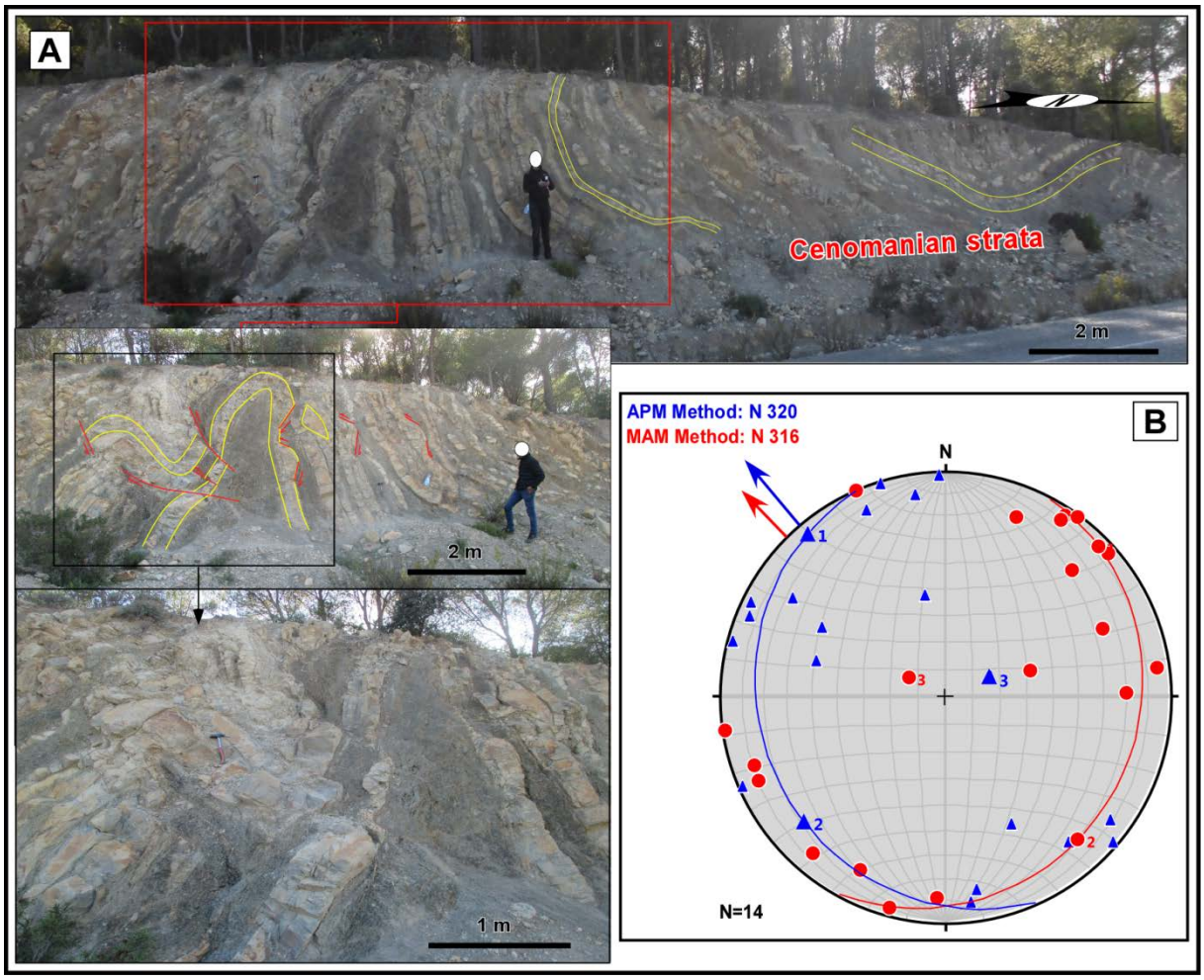

A
Cenomanian strata
2 m
2 m
1 m
B
APM Method: N 320
MAM Method: N 316
N
1
2
3
N=14

Fig.10

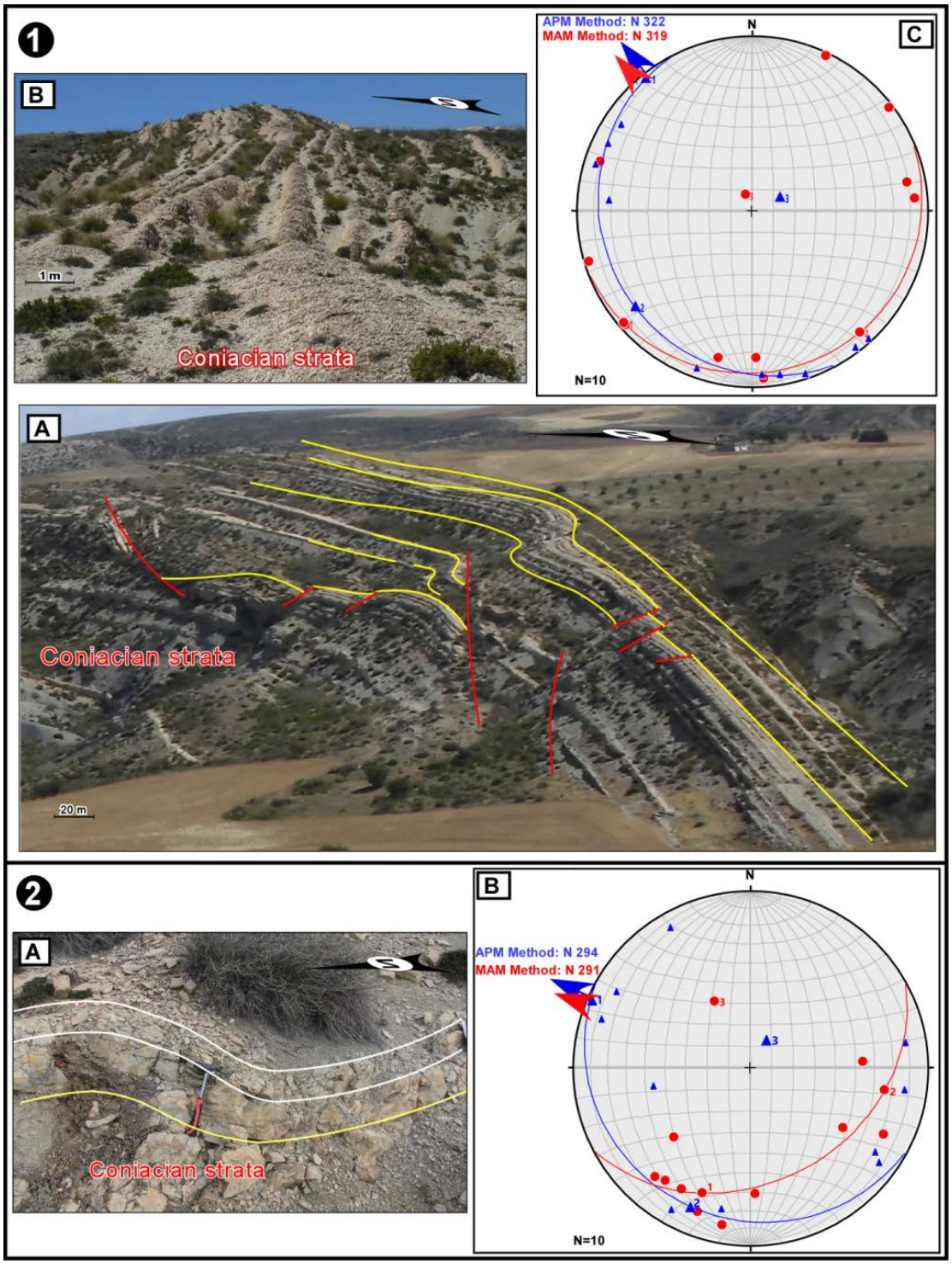

1
B
1 m
Coniacian strata
APM Method: N 322
MAM Method: N 319
N
C
N=10
A
Coniacian strata
20 m
2
A
Coniacian strata
B
APM Method: N 294
MAM Method: N 291
N
N=10

Fig.11

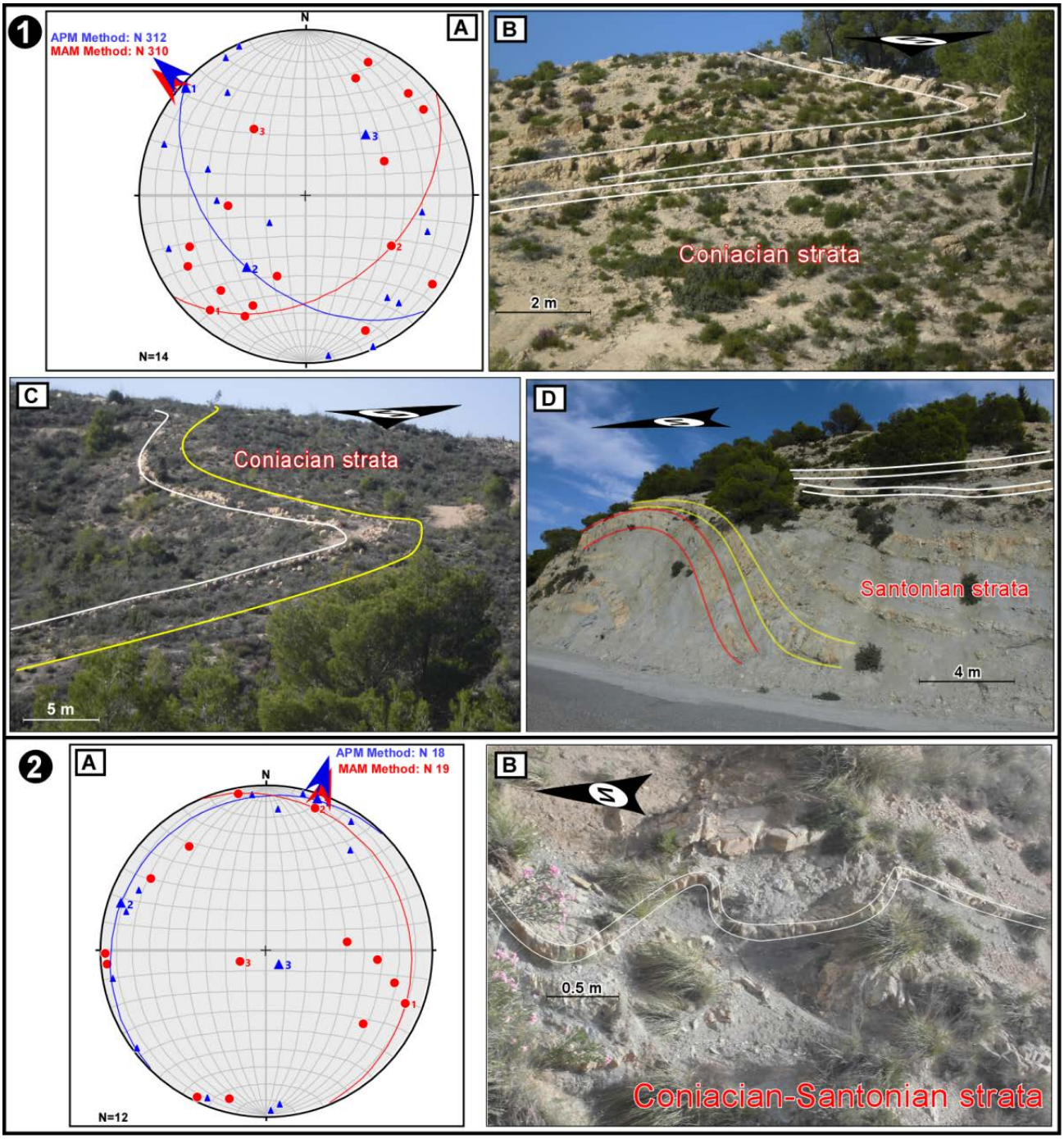

1
A
APM Method: N 312
MAM Method: N 310
N
N=14
B
Coniacian strata
2 m
C
Coniacian strata
5 m
D
Santonian strata
4 m
2
A
APM Method: N 18
MAM Method: N 19
N
N=12
B
0.5 m
Coniacian-Santonian strata

Fig.12

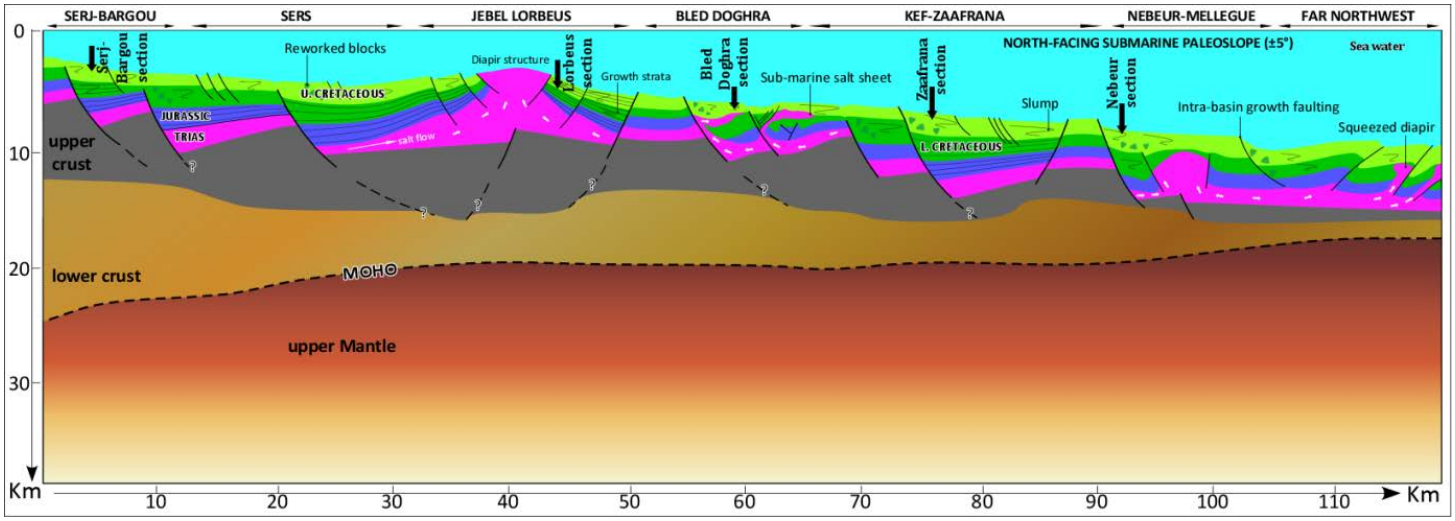

SERJ-BARGOU
SERS
JEBEL LORBEUS
BLED DOGHRA
KEF-ZAAFRANA
NEBEUR-MELLEGUE
FAR NORTHWEST
Serj-Bargou section
Reworked blocks
U. CRETACEOUS
JURASSIC
TRIAS
salt flow
Diapir structure
Lorbeus section
Growth strata
Bled Doghra section
Sub-marine salt sheet
Zaafrana section
NORTH-FACING SUBMARINE PALEOSLOPE (±5°)
Sea water
Slump
Nebeur section
Intra-basin growth faulting
Squeezed diapir
L. CRETACEOUS
upper crust
lower crust
MOHO
upper Mantle
0
10
20
30
Km
10
20
30
40
50
60
70
80
90
100
110
Km

Fig.13